https://doi.org/10.5194/egusphere-2026-3660
Preprint. Discussion started: 7 July 2026

A Decadal-Scale Perspective on PM_{10} Composition and its Variability Drivers at the Alpine High-Altitude Research Station Jungfraujoch

Julian Weng[1], Yufang Hao[1], Benjamin T. Brem[1], Tianqu Cui[1], Peeyush Khare[1,7], Lubna Dada[1], Kaspar R. Daellenbach[1], Sophie Darfeuil[2], Gaëlle Uzu[2], Jean-Luc Jaffrezo[2], Martin Steinbacher[3], Stefan Reimann[3], Thaleia Gkraikou[4], Konstantina Oikonomou[4], Jean Sciare[4], Martine Collaud Coen[5], Claudia Mohr[1,6], Andre S. H. Prévôt[1], Martin Gysel-Beer[1], Imad El Haddad[1], and Patrik Winiger[1]

[1]PSI Center for Energy and Environmental Sciences, 5232 Villigen PSI, Switzerland
[2]Université Grenoble Alpes, CNRS, INRAE, IRD, G-INP, IGE, 38000 Grenoble, France
[3]Swiss Federal Laboratories for Materials Science and Technology, Empa, 8600 Dübendorf, Switzerland
[4]Climate and Atmosphere Research Center, The Cyprus Institute, Nicosia, 2121, Cyprus
[5]Federal Office of Meteorology and Climatology, MeteoSwiss, 1530 Payerne, Switzerland
[6]Department of Environmental Systems Science, ETH Zurich, 8092 Zürich, Switzerland
[7]Now at: Institute of Climate and Energy Systems (ICE–3): Troposphere, Forschungszentrum Jülich, 52428 Jülich, Germany

Correspondence: Patrik Winiger (patrik.winiger@psi.ch)

Abstract.

Atmospheric aerosols in the free troposphere (FT) exert a disproportionate influence on climate forcing yet remain poorly constrained. Here, we present an 11-year (2011–2021) characterization of PM_{10} chemical composition at the High Altitude Research Station Jungfraujoch (3580 m above sea level), capturing both FT conditions and episodic planetary boundary layer intrusions (PBLi). We integrate long-term measurements of organic aerosol (OA), elemental carbon, sulfate, crustal elements, trace metals, and bulk and molecular-level organic composition with gas-phase observations and proxies for atmospheric transport and oxidative capacity to quantify the drivers of aerosol loading and composition. The concentrations of primary aerosol species, including metals and elemental carbon, are strongly controlled by episodic PBL-to-FT transport (~2-3-fold seasonal amplitude, e.g. ~0.15 to 0.3 $\mathrm{ng\,m^{-3}}$ for Pb). Secondary species, including sulfate and OA, also reflect PBLi impact, but their formation requires sustained oxidative processing, for which the atmospheric humidity ratio (ω) acts as a key control. OA exhibits the strongest seasonal amplitude (~10-fold, ~0.1 to 1 $\mathrm{\mu g\,m^{-3}}$), additionally reflecting enhanced biogenic emission intensities in the PBL. This is accompanied by a systematic shift in $\mathrm{C_9}$ and $\mathrm{C_{10}}$ compounds, likely related to seasonal maxima in monoterpene emissions. Together, these results demonstrate that FT aerosol is governed by a dynamic interplay between episodic PBL-to-FT transport, source emission intensities and oxidative processing. This dataset constrains their relative contributions, and provides decade-scale observational benchmarks for improving the representation of transport and aging in atmospheric models, with implications for reducing uncertainties in climate forcing.

https://doi.org/10.5194/egusphere-2026-3660
Preprint. Discussion started: 7 July 2026

1 Introduction

Atmospheric aerosols exert wide-ranging impacts on the Earth's climate system, modulating radiative forcing both directly, via scattering and absorption of solar radiation (Yu et al., 2006), and indirectly, by modification of cloud formation and lifetime (Lohmann and Feichter, 2005). While commonly studied near major emission sources in the planetary boundary layer (PBL) (Jimenez et al., 2009), aerosols in remote, high-altitude regions — particularly within the free troposphere (FT) — are of distinct and growing scientific interest. Lifetimes of FT aerosols can exceed those in the PBL by several orders of magnitude (Croft et al., 2014), redistributing aerosol burdens across continents and amplifying their climate impacts on synoptic scales (Bond et al., 2013; Kok et al., 2023). Concurrently, aerosol–climate interactions often exhibit a pronounced sensitivity to altitude: for example, the direct radiative forcing associated with black carbon is substantially enhanced in the FT relative to the PBL, particularly above clouds (Samset and Myhre, 2011; Zarzycki and Bond, 2010). An accurate representation of tropospheric aerosols in global climate models is therefore essential in order to reduce uncertainties of radiative forcing estimates and improve predictions of aerosol–climate feedbacks.

To asses the climate impact of aerosols, spatiotemporally resolved estimates of global aerosol burdens are provided by simulation models (Textor et al., 2006; Tsigaridis et al., 2014). These models typically integrate emission inventories of aerosols and their precursors with meteorological transport simulations, in conjunction with representations of aerosol microphysical processes and chemical transformation mechanisms. For remote locations like the FT, secondary aerosol formation (i.e. through oxidative reactions of volatile precursor gases followed by gas-to-particle conversion) is of key importance (Tsigaridis et al., 2014; Pai et al., 2020; Liu et al., 2021). In simplistic models, aerosol chemical aging is represented as homogeneous and heterogeneous oxidation driven by hydroxyl radicals (OH) (Jimenez et al., 2009), the predominant atmospheric oxidant, especially in clean environments like the FT (Yang et al., 2016; Stone et al., 2012; Lelieveld et al., 2016). The primary formation of OH occurs trough photodissociation of ozone (O_3) by UV light and reaction of excited state $O(^1D)$ with atmospheric water vapor (Stone et al., 2012):

$$O_3 + h\nu(\lambda < 320nm) -> O_2 + O(^1D) \quad \text{(R1)}$$

$$O(^1D) + H_2O -> 2OH \quad \text{(R2)}$$

Despite ongoing optimization efforts (Textor et al., 2006; Tsigaridis et al., 2014), contemporary aerosol simulations still exhibit substantial limitations in accurately reproducing both the magnitude and spatiotemporal variability of atmospheric aerosols. This is the case particularly for the chemically complex organic aerosol (OA) fraction (Heald et al., 2011; Pai et al., 2020; Liu et al., 2021) which is commonly dominating fine-mode PM in observations (Jimenez et al., 2009). The divergence between OA model predictions and *in-situ* data increases as photochemical age progresses in remote environments, reaching a maximum for the FT and long-range transported aerosols (Volkamer et al., 2006; Heald et al., 2011; Tsigaridis et al., 2014; Hodzic et al., 2020). The AeroCom II model intercomparison study yielded a diversity in the range of two orders of magnitudes

https://doi.org/10.5194/egusphere-2026-3660
Preprint. Discussion started: 7 July 2026

for OA concentrations in the FT (Tsigaridis et al., 2014). These high uncertainties propagate into climate models, for instance resulting in an order of magnitude variability of estimated secondary OA (SOA) radiative forcings (Spracklen et al., 2011; Myhre et al., 2013). The inadequate model performance in the FT is attributed to i) an insufficient understanding of aerosol transport, secondary aerosol formation and processing as well as ii) the limited availability of *in-situ* long-term observations in remote locations of the FT, which are a prerequisite for model evaluation and optimization (Tsigaridis et al., 2014).

High-altitude mountain observatories can serve as an ideal platform for mitigating observational limitations and addressing knowledge gaps related to tropospheric aerosols (Okamoto and Tanimoto, 2016). Unlike sporadic short-term airborne campaigns (Heald et al., 2011), mountain sites offer long-term data under stationary conditions, capturing seasonal variability and providing the means for process understanding (Collaud Coen et al., 2007, 2018; Moreno et al., 2024). Mountain ranges, moreover, are key drivers of vertical aerosol transport through thermal convection (mountain venting) and orographic lifting (Henne et al., 2004; Collaud Coen et al., 2011). High altitude observatories therefore lie at the interface of PBL and FT, providing information about background FT conditions and intermittent vertical transport from the PBL.

Here, we present a comprehensive characterization of the PM_{10} (particulate matter with aerodynamic diameter smaller than $10\,\mu\mathrm{m}$) chemical composition at the Alpine High Altitude Research Station Jungfraujoch (JFJ, $3580\,\mathrm{m}$ above sea level) over a period exceeding one decade (2011–2021). In a holistic approach, long-term aerosol constituent seasonalities are set into context with *in-situ* measurements of gas-phase composition as well as proxies for PBL-FT transport and the atmospheric oxidative capacity. This is complemented by a detailed characterization of water-soluble OA (WSOA) composition, using offline target and non-target mass spectrometry (MS) — Ion Chromatography-MS (IC-MS) and Ultra High Performance Liquid Chromatography-Tandem MS (UHPLC-MS/MS) as well as the aerosol mass spectrometer (AMS) and extractive electrospray ionization MS (EESI-MS). In combination, these measurements provide a comprehensive long-term dataset together with a detailed perspective on the interplay among atmospheric transport, emission seasonalities in the PBL, secondary aerosol formation, and aging processes for the aerosol in a remote environment located within, or at the transition to, the FT.

2 Experimental

2.1 Measurement site description

The High Altitude Research Station Jungfraujoch (JFJ, $3580\,\mathrm{m}$ above sea level, 46°32′ N 7°59′ E) is located on an exposed mountain ridge in the Swiss Alps. The observations are hosted in JFJ's Sphinx observatory, which was established in 1937 (Leuenberger and Flückiger, 2008). First semi-continuous aerosol observations were started in 1973 (Bukowiecki et al., 2016). While being far away from any major pollution sources, the JFJ is categorized as *mostly remote*, as the station experiences intermittent influences from Earth surface air fluxes (Henne et al., 2010; Collaud Coen et al., 2018). The contribution of local primary emissions to OA mass concentration at the JFJ lie between 7 to 12 %, predominantly associated to touristic activities (Fröhlich et al., 2015). Local influences on mean values of OA properties (as well as most other aerosol constituents) can therefore be considered minor, all year round.

https://doi.org/10.5194/egusphere-2026-3660
Preprint. Discussion started: 7 July 2026

The variability of aerosol observations at the JFJ is strongly impacted by meteorologically driven air mass transport (Baltensperger et al., 1997; Cozic et al., 2008). While generally situated in the FT, vertical transport leads to periodical intrusions of polluted PBL air masses (Collaud Coen et al., 2011). The intensity of vertical transport follows strong seasonal patterns with maxima from late spring to summer and minima in winter (Bukowiecki et al., 2016; Herrmann et al., 2015; Jurányi et al., 2011).

2.2 Aerosol sampling and sample selection

For the period from 2011 to 2021, daily 24 h High Volume (HiVol) PM_{10} filters were collected as part of the *Swiss National Air Pollution Monitoring Network* (NABEL) (Hueglin et al., 2024). Aerosol was sampled on quartz tissue filters (Pallflex XP56 Tissuquartz 2500QAT-UP, Cytiva, USA) using a HiVol sampler (DHA-80, Digitel, Switzerland) with a sample volume of 1075 m^3 per day. After initial filter conditioning at 20 °C and 50 % RH for 96 h, filters were stored at -23 °C until analysis. Gravimetric mass concentration of PM_{10} was determined by weighing the filters before and after sample collection with a high precision analytical balance with antistatic-kit (XP205, Mettler Toledo, USA) in NABEL's central laboratory close to Zurich. Along with the ambient samples, fieldblank filters were collected that were treated identically (including transport to the JFJ) except for exposure to filtration in the HiVol sampler.

For chemical analysis, filters for the time period between 2011 and 2021 were pooled into composites of four at an interval of four days each (cf. the schematic in Fig. S1; note that for plotting, always the earliest filter sampling date is used). A statistical justification for this approach is provided in Sect. S1.1. Comparison of 16-day averaged sulfate mass concentrations with the composite means (every 4th day of 16 days) shows good agreement ($R^2 = 0.64$, root-mean-square error $< 10\,\%$ of average, Fig. S2). For this study, data of samples dominated by long-range transported Saharan dust conditions at the JFJ were omitted (overall 43 out of 249 composite samples). This is because such filters are subject to strongly elevated aerosol loadings of dust constituents, while other aerosol and gas-phase properties could also be impacted. Saharan dust events at the JFJ are detected by online *in-situ* optical methods (Collaud Coen et al., 2004, 2026) and eventually filtered by a elemental titanium concentration threshold (Sect. S1.2 and S1.3). A detailed description of the Saharan dust data filtering and applied thresholds is provided in Sect. S1.3 and Fig. S3.

2.3 Chemical analysis of PM_{10} filter samples

Bulk organic carbon (OC) and elemental carbon (EC) ambient concentrations were measured for the time periods from August 2013 to September 2014 and March 2019 to November 2019 by a thermal-optical OC/EC-analyzer (Model 5, Sunset Lab, USA) using the European Supersites for Atmospheric Aerosol Research (EUSAAR-2) protocol (Cavalli et al., 2010). For this, daily resolution filter samples were analyzed and averaged for the composite sample time periods. Bulk water-soluble organic carbon (WSOC) ambient concentrations were obtained from analysis of composite filter sample water extracts by a total organic carbon analyzer (TOC-L-series, Shimadzu, Japan), using the system's *non-purgeable organic carbon* protocol (Cui et al., 2024). The same water extracts were used for non-target analysis of bulk organic composition by Offline Long Time-of-Flight Aerosol Mass Spectrometry (Offline-AMS, Aerodyne, USA), also providing WSOA ambient concentrations and organic matter/organic

https://doi.org/10.5194/egusphere-2026-3660
Preprint. Discussion started: 7 July 2026

carbon (OM/OC) ratios (Daellenbach et al., 2016). Concurrently, from the same water extracts, near-molecular-resolution composition of WSOA was obtained from Offline Long Time-of-Flight Extractive Electrospray Ionization Mass Spectrometry (Offline-EESI-MS, custom-designed inlet (Lopez-Hilfiker et al., 2019), mass spectrometer from TOFWERK, Switzerland) (Cui et al., 2024; Hao et al., 2025). Independently, water extracts from other aliquots of the same filters were used to obtain ambient concentrations of individual inorganic and organic compounds. A range of inorganic ions (including sulfate and ammonium) as well as organic carboxylic and dicarboxylic acids were measured by Ion Chromatography-Mass Spectrometry (IC-MS, INTEGRION and ISQ EC, Thermo Fisher Scientific, USA). A selection of sugars and sugar alcohols were analyzed by a recently developed method based on Ultra High Performance Liquid Chromatography-Tandem Mass Spectrometry (UHPLC-MS/MS, ExionLC AD binary pump and 5500 QTRAP, Sciex, USA) (Bros et al., 2025). Metals and elements were quantified on another aliquot of the same filters based on Inductively Coupled Plasma Mass Spectrometry (ICP-MS, iCAP TQ ICPMS, Thermo Fisher Scientific, USA), applying a soft digestion method (without hydrofluoric acid) for sample preparation. Details on sample preparation, analytical procedures, instrumental specifications and data analysis workflows can be found in Sect. S2. A cross-validation of the various independent analysis methods is provided in Sect. S3, demonstrating good agreement and combined uncertainties related to sample preparation and measurements of below 15 %.

2.4 Online *in-situ* measurement of gas- and aerosol-phase properties

A suite of gas-phase and aerosol properties was measured online *in-situ* at the JFJ. Unless stated otherwise, all parameters were temporally aggregated over the same time periods as the composite filter samples. The measurements were conducted as part of the NABEL, the *Global Atmosphere Watch* (GAW) program and the Swiss contribution to the *Aerosol, Clouds and Trace Gases Research Infrastructure* (ACTRIS-Switzerland).

A heated inlet (20 °C) with losses below 5 % for accumulation-mode particles was used for all online aerosol instruments (Weingartner et al., 1999). Online PM mass concentrations (PM_1, PM_{10}) were measured by a fine dust monitor (FIDAS 200, PALAS, Germany, Sect. S4). A good correlation of FIDAS PM_{10} and gravimetric PM_{10} is observed ($R^2 = 0.94$, Fig. S10). For quantification, FIDAS PM_1 and PM_{10} raw data are referenced to the gravimetric PM_{10}, as described in Sect. S4. Equivalent black carbon (eBC) concentrations were obtained from online aerosol absorption measurements by a multi-angle absorption photometer (MAAP, 5012, Thermo Fisher Scientific, USA) at effectively 637 nm. The conversion of instrument derived absorption coefficients to eBC was performed using the ACTRIS-harmonized mass absorption cross-section (MAC) of $10\,\mathrm{m^2\,g^{-1}}$, as described in Sect. S5 and Zanatta et al. (2016). A comparison of eBC with EC shows a good relative agreement ($R^2 = 0.64$, Fig. S11), but a slight overestimation of retrieved eBC (simple linear regression $SLR\ slope = 0.84$), likely related to an underestimated site-specific MAC due to lensing effects in summer (cf. Sect. S5).

The trace gas species NO_x, O_3 and SO_2 were measured online by different gas monitors as explained in Sect. S6. A range of non-methane hydrocarbons (NMHCs) and halogenated VOCs were quantified on-site by semi-continuous Medusa cold trap gas-chromatography mass spectrometry (GC-MS). Further information on Medusa GC-MS measurements is provided in Sect. S7.

https://doi.org/10.5194/egusphere-2026-3660
Preprint. Discussion started: 7 July 2026

3 Tracer-based proxies for planetary boundary layer intrusions, the humidity ratio ω as a proxy for atmospheric oxidative capacity and their mutual relationship

PBL intrusions (PBLi) through regional vertical transport to the JFJ can be quantified by different PBLi tracers (Herrmann et al., 2015). These are compounds with strong and constant emission sources close to the Earth's surface, in combination with well-constrained, short atmospheric lifetimes following their release. For this study, three independent tracers were compared: i) the ratio between reactive nitrogen species in both gas and particle phase (NO_y) and carbon monoxide NO_y/CO [ppb/ppb] (Zellweger et al., 2003); while NO_y is removed through photochemical processing followed by wet deposition, the more inert CO accounts for dilution effects; ii) concentrations of radon-222 (^{222}Rn) which is emitted naturally from land surfaces and has a radioactive half-life of about 4 days (Griffiths et al., 2014); and iii) the number concentration of accumulation mode particles above 90 nm (N_{90}), as under FT conditions, no substantial number of accumulation-mode particles is present at the JFJ (Herrmann et al., 2015). Details on online measurement and data coverage of these parameters are provided in Sect. S9.1.

In the absence of other parameters, also the humidity ratio ω has been used as a tracer for PBLi in individual case studies at the JFJ (Zellweger et al., 2003) and other high altitude sites (Ambrose et al., 2011; Obrist et al., 2008; Zografou et al., 2025). ω is a metric for the mass of water vapor per unit mass of dry air (expressed as g of water vapor per kg of dry air). The origin of atmospheric water vapor is attributed to surface evaporation in the PBL (Jin et al., 2024). For this study, ω was obtained from the meteorological parameters temperature, relative humidity (RH) and barometric pressure measured at the JFJ (cf. Sect. S8.1 for measurement details). A parameterization according to Buck was applied to estimate saturation vapor pressures at different temperatures (Buck, 1981). The consecutive calculation steps are described in detail in Sect. S8.2. During air mass transport from the PBL to the FT, ω can generally be considered a conservative property of the respective air mass (it is independent to changes in temperature or pressure), with exception of water removal through strong precipitation events (Henne et al., 2005).

In this study, the mutual impact of PBLi and oxidative processing on gas-phase and aerosols constituents is investigated. In that context, the variable ω is introduced as a proxy for the atmospheric oxidative capacity history of PBLi air masses prior to arrival at the JFJ (Sect. 4.2). To disentangle the respective roles of transport (PBLi) and oxidative processing, the covariances of ω and different PBLi tracers were analyzed in detail in Sect. S9.2. This is especially relevant given that the origin of water vapor in tropospheric altitudes is associated with vertical transport from the PBL (Henne et al., 2005). From long-term, high-temporal resolution online data it can be concluded that elevated PBLi tracers are conditional for high ω at the JFJ, consistent with the attribution of water vapor to surface evaporation in the PBL. However, scatter plots of ω and a range of species with strong association to the PBL, including NO_y/CO, ^{222}Rn, NO_x, NO_y (Fig. S17) as well as eBC and C_2Cl_4 (Fig. 18), illustrate that at moderate and strong PBLi, high ω is not exclusive. On the contrary, a broad distribution of ω is observed even at strong PBLi, including conditions with low ω. Consequently, similar values of ω observed at the JFJ can correspond to substantially different levels of PBLi strength, reflecting, for example, seasonal variability in surface evaporation and associated water vapor supply. This behavior is underlined by statistical analyses, applying Mann-Whitney-U-tests of binned ω with respect to the PBL associated species (Fig. S19) , as well as a quantile regression for ω with respect to the PBLi tracers NO_y/CO and ^{222}Rn,

https://doi.org/10.5194/egusphere-2026-3660
Preprint. Discussion started: 7 July 2026

as described in detail in Sect. S9.2. In conclusion, PBLi tracers and ω are only partly covariant at the JFJ, providing the means for an independent assessment of their respective influences on gas- and aerosol-phase constituents.

For selection of a robust proxy for PBLi, the PBLi tracers NO_y/CO, ^{222}Rn and N_{90} were compared using scatter plots colored according to ω (Fig. S21). NO_y/CO and ^{222}Rn show a linear relationship, independent of ω (Fig. S21a). In contrast, the relationships of NO_y/CO or ^{222}Rn with N_{90} are highly conditional on ω (Fig. S21b and c). N_{90} represents exclusively the aerosol phase, which can be subject to changing sources, oxidative processing and microphysical phase-transitioning. NO_y includes a broad range of reactive nitrogen species in both gas and particle phase, therefore remaining indifferent to oxidation and phase-transitioning of compounds. Consequently, the PBLi tracer chosen for evaluations in this study is NO_y/CO. All trends are also observed independently for ^{222}Rn, which was not selected due to its shorter data coverage and lower dynamic range.

4 Results and Discussion

4.1 Fine- and coarse-mode aerosols with comparable annual mass but variable seasonalities at high altitude

Figure 1a shows the 11-year time series (2011-2021) of gravimetric PM_{10} and the major PM_{10} constituents at the JFJ. Particulate nitrate was excluded due to known biases in filter-based nitrate quantification arising from evaporative losses (Chow et al., 2005). Online measurements at the JFJ, however, have shown that the nitrate fraction in PM_1 aerosol remains below 10 % all year round and is therefore of very minor contribution (Fröhlich et al., 2015). All aerosol constituents in Fig. 1a show a pronounced seasonal variability, characterized by elevated mass concentrations typically during spring and summer and distinct minima in winter. These seasonal patterns are in line with trends reported previously for a range of aerosol properties at the JFJ, from total suspended PM (Baltensperger et al., 1997) over optical properties (Collaud Coen et al., 2011), size distributions (Herrmann et al., 2015), chemical composition (Fröhlich et al., 2015) to cloud condensation nuclei number concentrations (Jurányi et al., 2011). Already in the late 1990s, this pattern has been attributed to seasonal differences in vertical pollution transport from the PBL (Baltensperger et al., 1997).

Comparison of the mass concentrations in Fig. 1a with the co-located fine dust monitor FIDAS reveals that PM_1 is very well explained by the sum of WSOA, sulfate and ammonium ($SLR\ slope = 1.1$, $R^2 = 0.93$, cf. Fig. S22). Consequently, these components represent the fine-mode aerosol (below 1 µm) at the JFJ, along with EC (or eBC) and nitrate, which both are present at low concentrations. Median OC/EC ratios lie well above 10 in summer and are lower in autumn and winter (median between 4 and 7, Fig. S23). The strong dominance of OC over EC is characteristic for remote high altitude environments with highly aged aerosol profiles and strong contribution of secondary constituents (Timonen et al., 2014; Moreno et al., 2024; Putaud et al., 2025). Consistent with pronounced aerosol aging is also the very high OA water solubility (83 % of OC, cf. Sect. S10.3 and Fig. S24).

The remaining fraction of gravimetric PM_{10} (named PM_{10} Residual in Fig. 1) agrees well with coarse-mode aerosol (i.e. PM_{1-10}) from FIDAS measurements ($SLR\ slope = 0.82$, $R^2 = 0.64$, cf. Fig. S25a and b). This fraction is primarily composed of (regionally transported) mineral dust, based on i) its good correlation with a sum of the typical crustal ions

https://doi.org/10.5194/egusphere-2026-3660
Preprint. Discussion started: 7 July 2026

Ca^{2+}, Mg^{2+} and K^+ (from IC-MS, $R^2 = 0.54$, cf. Fig. S25a and c), and ii) mass closure with mineral dust and trace element estimates (calculated from ICP-MS, $median\ recovery = 0.93\ with\ IQR = 0.80\ to\ 1.0$, cf. Sect. S10.5 and Fig. S26). Only a small fraction of samples ($< 10\,\%$) are identified where mineral dust alone cannot account for the PM_{10} Residual, indicating that contributions from other coarse-mode species occur very sporadically. A typical coarse-mode aerosol composition at the JFJ (excluding Saharan dust conditions) is presented in Fig. S27.

On an annual basis, cumulative fine- and coarse-mode aerosol masses are of comparable magnitude at the JFJ (Σ mass fine mode/ Σ PM_{10} Residual $= 0.64$, excluding Saharan dust). However, while all constituents show a pronounced seasonality, their relative contribution to PM_{10} differs considerably over the year. As shown by the mass fractions in Fig. 1b, the mostly coarse-mode PM_{10} Residual strongly dominates PM_{10} in winter, whereas the fine-mode fraction prevails towards summer. Consistent with previous online *in-situ* studies (Fröhlich et al., 2015), OA concentrations exceed sulfate in summer by a factor of 2 or more, while winter fractions are almost equal. Distinct differences in seasonalities are also observed for other PM_{10} constituents. The box plots in Fig. 2a to c show seasonal mass concentrations of the fine-mode constituents WSOA and sulfate as well as the representative coarse-mode species Ca^{2+}, Mg^{2+} and K^+. Fig. 2d displays the same for lead (Pb), a metal that is predominantly associated to the fine-mode aerosol fraction (Hueglin et al., 2005), originating mainly from industrial emissions (and traffic) in the PBL (European Environment Agency, 2022). The yearly cycles of sulfate and especially WSOA exhibit a high dynamic range, with median enhancements of around 4 and > 10 between winter and summer time. Also, summer concentrations predominate clearly over spring in both cases. In contrast, seasonalities are much more leveled for Ca^{2+}, Mg^{2+} and K^+ as well as for Pb. Median enhancements of mass concentrations in summer compared to winter are in the range of a factor 2 to 3, while there is no distinction between spring and summer. Consistent behaviors are also observed for other metal species like lithium, aluminum (commonly associated to coarse-mode (Hueglin et al., 2005; Wang et al., 2007), Fig. S28a and b) as well as cadmium and vanadium (commonly associated to fine-mode (Hueglin et al., 2005; Shafer et al., 2012; Allen et al., 2001), Fig. S28c and d). On a bulk aerosol level, the fine-mode PM_1 follows the trends of WSOA and sulfate, while the coarse-mode PM_{10} Residual exhibits less pronounced and more even seasonalities, like the metal species (Fig. S29).

A comparison with trends of the PBLi tracers NO_y/CO and ^{222}Rn (Fig. S16a and b) reveals that metal and coarse-mode species closely follow the seasonal variability of vertical air mass transport strength. Apart from the comparatively modest enhancement of NO_y/CO and ^{222}Rn in summer relative to winter (~2-fold), they exhibit similar characteristics, with spring and summer levels being approximately equal. Unsurprisingly, the particle number concentration N_{90}, being strongly associated with accumulation-mode particles, closely follows the more pronounced enhancements of fine-mode aerosol and shows a distinct summer maximum (Fig. S16c).

In the following, we investigate to what extent drivers in addition to vertical transport explain aerosol concentrations and the pronounced seasonalities, especially of fine-mode species, at high-altitude sites like the JFJ.

https://doi.org/10.5194/egusphere-2026-3660
Preprint. Discussion started: 7 July 2026

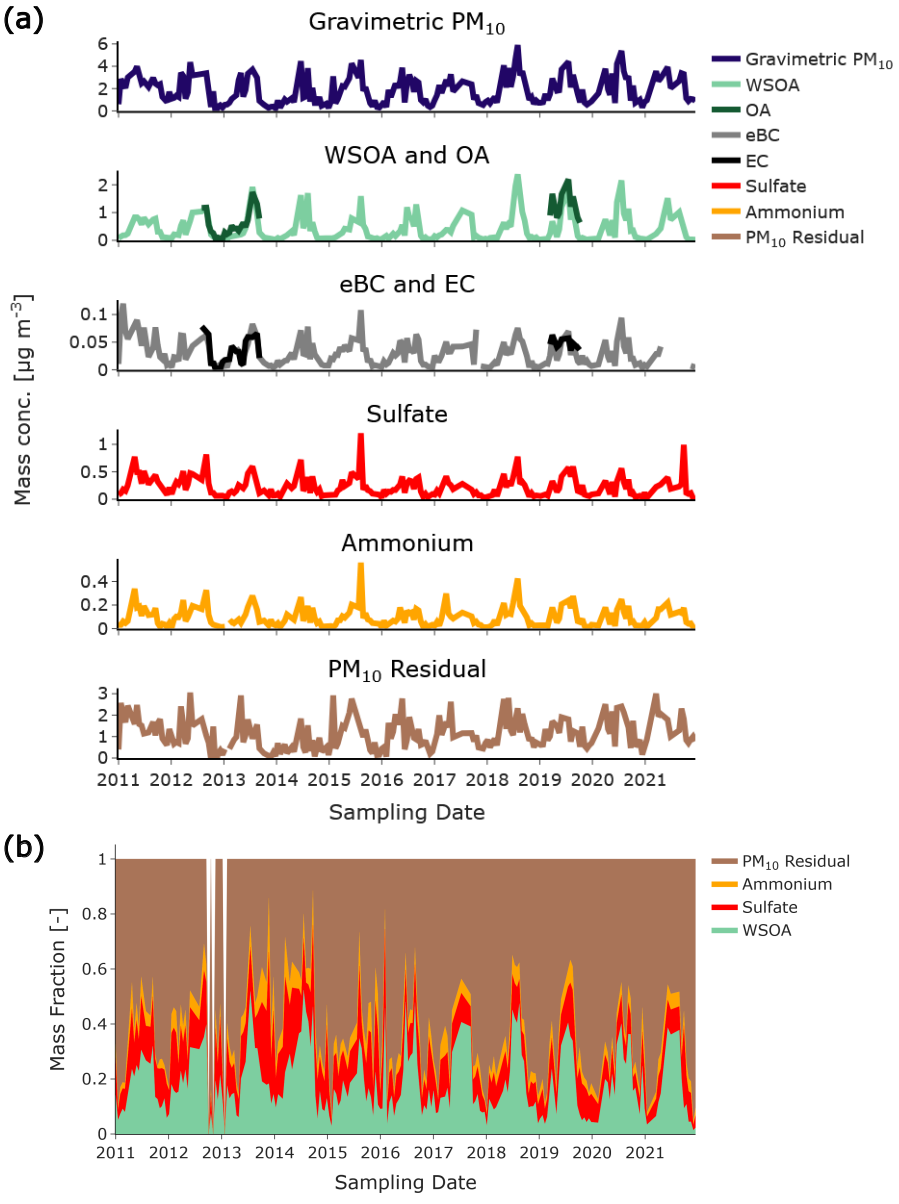

Figure 1. (a) Time series of gravimetric PM_{10} and different PM_{10} constituent mass concentrations at the JFJ from 2011 to 2021. PM_{10} Residual was calculated by subtraction of WSOA, sulfate and ammonium from gravimetric PM_{10}. Besides minor contributions from nitrate, water-insoluble organic matter and trace elements, the PM_{10} Residual is predominantly composed of (regionally transported) mineral dust. (b) PM_{10} mass fractions of the major constituents (eBC is not included due to missing data points and its negligible contribution). Missing data points are depicted as white sections. Sampling dates dominated by Saharan dust were omitted from all plots.

https://doi.org/10.5194/egusphere-2026-3660
Preprint. Discussion started: 7 July 2026

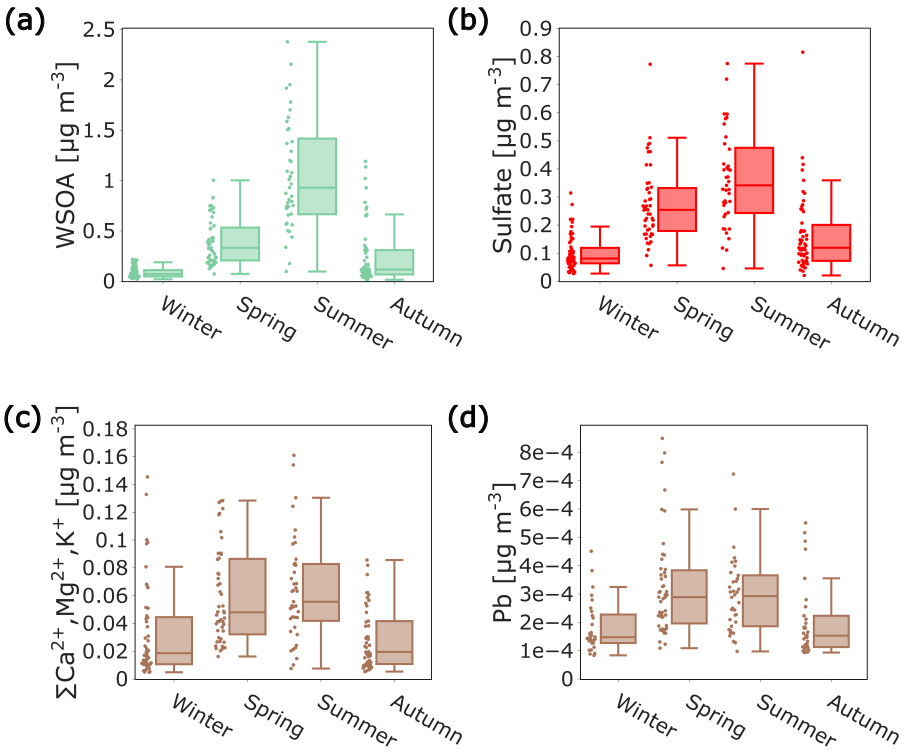

Figure 2. Seasonal trends of different PM_{10} constituent mass concentrations: (a) WSOA, (b) sulfate, (c) the sum of Ca^{2+}, Mg^{2+} and K^{+} and (d) Pb. Seasons are defined as Winter - DJF, Spring - MAM, Summer - JJA, Autumn - SON. Sampling dates dominated by Saharan dust were omitted from all plots. For Pb, some winter values of later years are below the limits of quantification; however, observations from the earlier years confirm that the seasonal amplitude, especially between winter and spring/summer, ranges by a factor of 2 to 3.

4.2 How the atmospheric oxidative capacity — captured by the humidity ratio ω — shapes the fate of trace gases and VOCs at a high altitude receptor side

Among the factors controlling aerosol concentrations, the atmospheric oxidative capacity is particularly relevant for remote regions, where the fraction of secondary aerosol becomes increasingly important (Tsigaridis et al., 2014; Hodzic et al., 2020). In Fig. 2, the seasonal patterns particularly of OA and sulfate deviate strongly from those of the PBLi tracers (Fig. S16). Unlike for the primary metals, OA can have strong contributions from secondary formation (Jimenez et al., 2009), and non-sea-salt sulfate (which dominates in continental Europe (Viana et al., 2014)) is almost exclusively formed by secondary pathways (Ye et al., 2023).

To account for the role of secondary aerosol formation, the variability in the atmospheric oxidative capacity history of an air mass — i.e. the oxidative capacity it experiences along the transport from the emission region to the JFJ — is represented in this study by a proxy, the humidity ratio ω. As shown in Eq. (R1) and Eq. (R2), the production rate of OH — which dominates the atmospheric oxidative capacity (Rohrer et al., 2014; Lelieveld et al., 2016; Price et al., 2025) — is a factor of O_3 mixing

https://doi.org/10.5194/egusphere-2026-3660
Preprint. Discussion started: 7 July 2026

ratios, UV radiation intensity (actinic flux) and water vapor concentrations, i.e. ω. While the seasonal O_3 variability at the JFJ is relatively low over the year (factor ~1.2 between winter and summer on average, Fig. S14a), the fluctuation of ω is large and characterized by a pronounced summer peak, exceeding spring and winter median values by factors of ~2 and ~3, respectively (Fig. S14c). Also global radiation intensities (which include the shortwave UV) show a high dynamic range, yet comparable spring and summer intensities (Fig. S14b). Although actinic flux is a key factor in OH production, it will be demonstrated here, based on the influence of ω on gas-phase composition, that the variability in OH exposure, and thus the atmospheric oxidative capacity history, is to a large extent represented by the proxy ω for the JFJ.

The influence of ω on gas-phase composition is evident from reactive nitrogen partitioning (Fig. 3a). While NO_y — originating almost exclusively from the PBL (Zellweger et al., 2003) — increases with transport strength, the fraction of NO_x (= $NO + NO_2$) within NO_y decreases systematically with increasing ω (cf. the binned local median trend lines of ω in Fig. 3a). At elevated NO_y, NO_x spans a wide range (from 0.2 to 1 ppb), but shows a clear negative dependence on ω, reflecting progressive oxidation of NO_x into more oxidized species such as HNO_3, particulate nitrate or peroxyacetyl nitrate (O'Brien et al., 1979; Zellweger et al., 2000). Thus, NO_x/NO_y provides an independent measure of photochemical aging (Zellweger et al., 2003) that is consistent with increasing OH exposure at high ω. Consistently, CO, whose primary atmospheric sink is oxidation by OH (Zheng et al., 2019), exhibits a moderate decrease at high ω (cf. the binned local median trend lines in Fig. 3b). O_3 on the other side increases moderately (cf. the binned local median trend lines in Fig. 3c), consistent with net photochemical production through NO_x-mediated oxidation of CO, CH_4, and VOCs (Lelieveld et al., 2016; Zanis et al., 2000). O_3 maxima in late spring at the JFJ have already previously been related to photochemical activity under presence of high NO_x from PBLi (Zanis et al., 2000; Schuepbach et al., 2001).

Concurrently, impacts of ω on the mixing ratios of different NMHCs and halogenated VOCs are observed (Fig. 4 and additional VOCs in Fig. S30). For all compounds, a clear negative correlation between ω and VOC mixing ratios is evident, independent of PBLi (i.e. NO_y/CO). That is even the case for species with a clearly traceable PBLi influence in their mixing ratios, like tetrachloroethylene, trichloroethylene or toluene, which all correlate well with NO_y/CO. Just as for NO_x, these trends can be attributed to oxidative depletion under high OH exposure. Importantly, at comparable levels of PBLi, VOC mixing ratios span a wide range depending on ω. Under low ω conditions, elevated VOC concentrations reflect efficient transport of polluted air masses from the PBL. Under high ω, however, oxidative depletion dominates, offsetting or even reversing the effect of transport. As a result, many anthropogenic VOCs exhibit seasonal cycles opposite to those of aerosol species at the JFJ, with maxima in winter and minima in summer (Fig. S31), consistent with previous observations (Legreid et al., 2008). These results establish a clear separation between transport-driven variability (captured by NO_y/CO) and chemistry-driven variability (captured by ω).

Together, the observations demonstrate that ω captures the cumulative oxidative processing experienced by air masses prior to arrival at JFJ. The strong and systematic dependence of gas-phase composition on ω validates its use as a proxy for atmospheric oxidative capacity. Simultaneously, it establishes plausibility for oxidative processing being a key determinant for the formation and seasonal evolution of secondary aerosol components in the FT.

https://doi.org/10.5194/egusphere-2026-3660
Preprint. Discussion started: 7 July 2026

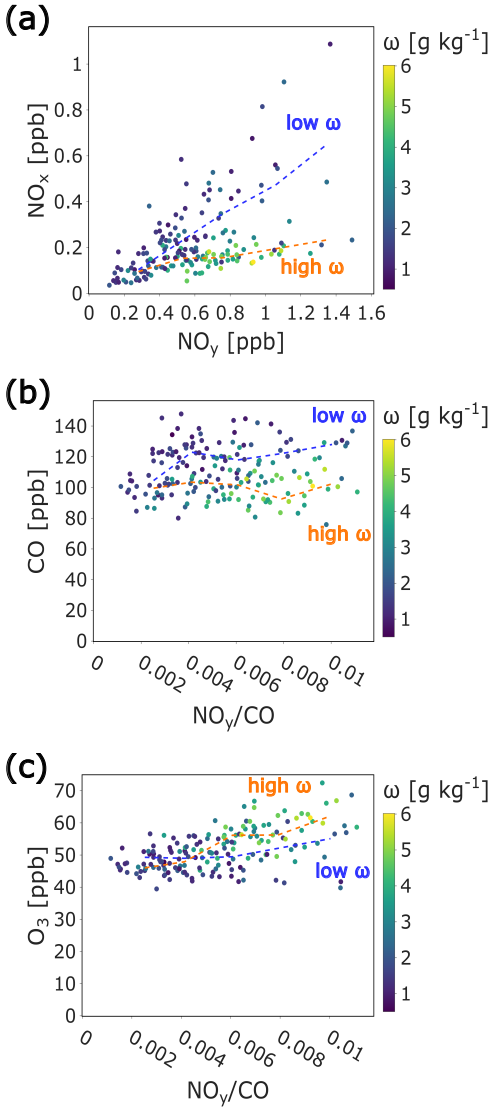

Figure 3. (a) Mixing ratio of NO_x as a function of NO_y at the JFJ, colored by ω. (b) Mixing ratio of CO and (c) O_3 as a function of NO_y/CO at the JFJ, colored by ω. Binned local median trend lines of mixing ratios vs. NO_x or NO_y/CO for low (blue) and high (orange) ω are displayed. For this, data were stratified into five discrete NO_y or NO_y/CO bins, locally segregated by the upper/lower half of ω observations and the medians for the low and high ω groups were calculated to obtain trend lines. Depicted are averages of high time resolution data, aggregated for the same time periods as the composite samples chemically analyzed in this study. Sampling dates dominated by Saharan dust were omitted from all plots.

https://doi.org/10.5194/egusphere-2026-3660
Preprint. Discussion started: 7 July 2026

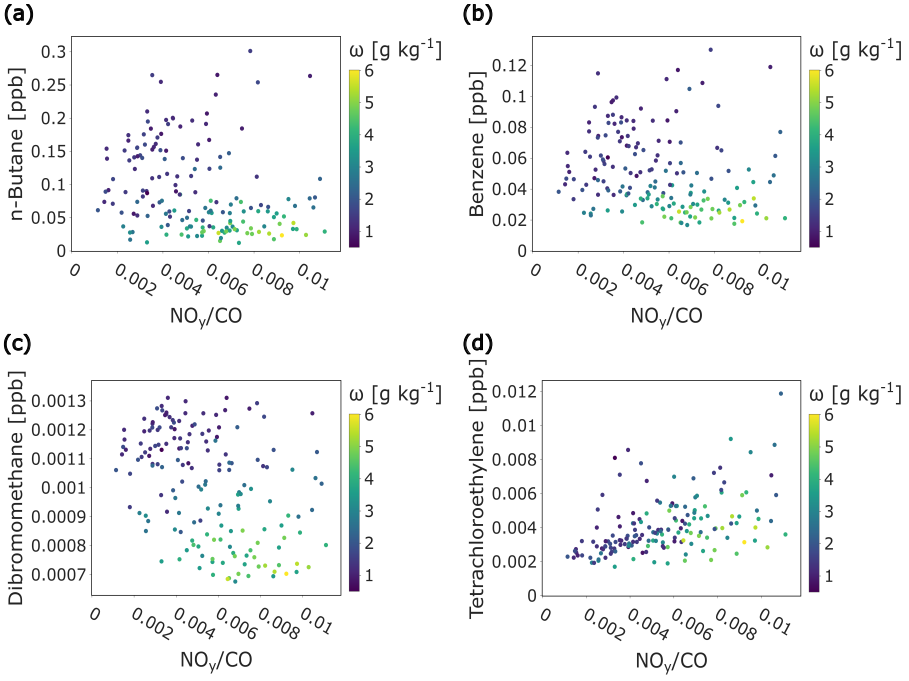

Figure 4. Mixing ratios of (a) *n*-butane, (b) benzene, (c) dibromomethane and (d) tetrachloroethylene as a function of the PBLi tracer NO_y/CO at the JFJ, colored by ω. Depicted are average data for the same time periods as the composite samples chemically analyzed in this study. Sampling dates dominated by Saharan dust were omitted from all plots.

4.3 The interplay of vertical transport, PBL emission intensities and atmospheric oxidative capacity as drivers of fine-mode aerosol concentrations at high altitude

Aerosol concentrations at high altitude emerge from a complex interplay of vertical transport, chemical reactivity, and PBL composition, which is itself modulated by variable emissions of aerosols and VOC precursors. Here, the seasonal variability of aerosol constituents is examined within this framework.

One way to isolate the impact of vertical transport is by comparing the behavior of the primary species eBC with the predominantly secondary bulk PM_1 as a function of atmospheric oxidative capacity, represented by ω (Fig. 5). eBC exhibits modest seasonal variability in the Swiss PBL (Hueglin et al., 2005) and remains largely inert to oxidative processing. Both eBC and PM_1 are clearly associated to sources in the PBL and only data satisfying a distinct PBL-to-FT association ($NO_y/CO > 0.004$, according to Fröhlich et al. (2015)) were included in Fig. 5. Median PM_1/eBC more than doubles from low to high ω levels, and elevated ratios occur across the full NO_y/CO-range, demonstrating independence from PBLi strength (Fig. S32).

Examining PM_1 and eBC individually confirms their distinct sensitivities (Fig. S33 and Fig. S34). Both correlate with PBLi; however, when linear fits are binned by ω, divergent behavior emerges. eBC slopes against NO_y/CO remain nearly constant

https://doi.org/10.5194/egusphere-2026-3660
Preprint. Discussion started: 7 July 2026

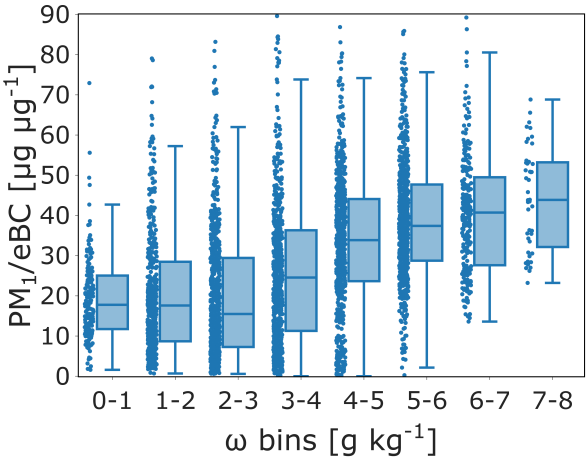

Figure 5. The ratio of PM_1/eBC at the JFJ, presented as box plots for different discrete ω bins. Only data points with a $\mathrm{NO_y/CO}$ above a threshold value of 0.004 were included, to assure considerable influence from PBLi and so a clear source-receptor relationship between emission in the PBL and transport to the JFJ. PM_1 data is from online FIDAS measurements. Data points are 3 h aggregated averages of the whole period between November 2016 and February 2020. Sampling dates dominated by Saharan dust were omitted based on flags obtained from optical data available at high time resolution.

across ω bins, reflecting its inert nature. In contrast, PM_1 exhibits a steepening slope with increasing ω, rising fivefold as ω increases from 1 to 8 $\mathrm{g\,m^{-3}}$, indicating synergistic amplification of fine-mode aerosol.

These observations highlight a general trend: while eBC remains largely independent of ω, PM_1 is strongly modulated by ω, superimposed on PBLi effects. Two complementary mechanisms likely contribute: i) an enhanced secondary aerosol formation within the PBL and along the transport pathway to the JFJ, driven by increased atmospheric oxidative capacity; and ii) co-variation of ω with PBL temperatures and seasons, which govern emission strengths of biogenic primary aerosols and biogenic SOA precursor VOCs (Samaké et al., 2019; Sporre et al., 2019).

A clearer differentiation of these complementary effects can be gained by analyzing individual aerosol constituents: the predominantly secondary WSOA and sulfate, as well as the primary Pb. All of these species show a strong dependency on PBLi, indicated by their correlation with $\mathrm{NO_y/CO}$ (Fig. 6). However, the superimposed ω-dependence differs markedly (cf. the binned local median trend lines of ω in Fig. 6): Pb remains largely independent of ω, sulfate shows moderate ω-sensitivity, and WSOA exhibits the strongest dependence, increasing fivefold at $\omega > 3\,\mathrm{g\,m^{-3}}$ compared to $\omega < 3\,\mathrm{g\,m^{-3}}$. Remarkably, under low ω-conditions, even strong PBLi episodes yield only modest WSOA and sulfate enhancements relative to FT background conditions. The differences in sulfate and WSOA behaviors suggest two implications: i) the correlation of sulfate with ω highlights the role of oxidative capacity independent of PBL composition effects. The emission strength of the sulfate precursor $\mathrm{SO_2}$ is not correlated with PBL temperature. In fact, $\mathrm{SO_2}$ mixing ratios peak in spring time at the JFJ and sulfate concentrations at different PBLi are much better explained by ω than by $\mathrm{SO_2}$ mixing ratios (Fig. S35); and ii) the even stronger correlation of WSOA with ω suggests that for OA, indeed overlapping effects of biogenic aerosol (precursor) emission strengths and

https://doi.org/10.5194/egusphere-2026-3660
Preprint. Discussion started: 7 July 2026

oxidative reactivity are at play. These considerations apply not only for the species presented in Fig. 6, but a variety of typical secondary (e.g. elemental S and Se, cf. Fig. S36) and primary (e.g. elemental Cd, Li, Al, sum of Ca^{2+}, Mg^{2+} and K^{+}, cf. Fig. S37) aerosol constituents as well as the bulk fine- and coarse-mode PM at the JFJ (Fig. S38).

In summary, the seasonal cycles of aerosol constituents at the JFJ (Sect. 4.1) are consistently explained by PBLi strength, atmospheric oxidative capacity, and seasonally varying biogenic emission strengths in the PBL. Secondary species and consequentially the fine-mode bulk PM, are following seasonal cycles of atmospheric oxidative capacity, likely intensified by correlating PBL emission intensities. As previously reported (Baltensperger et al., 1997), PBLi remains the driver of pollution transport to the JFJ and hence is conditional for elevated aerosol concentrations. Concurrently, other parameters — most notably the atmospheric oxidative capacity — ultimately govern how PBLi episodes reflect in both gas and aerosol phase.

4.4 Molecular constraints on the role of atmospheric oxidative capacity in SOA reactivity

Enhanced biogenic emissions within the PBL and variations in atmospheric oxidative capacity likely both contribute to summertime maxima of OA concentrations observed at the JFJ. Disentangling the respective contributions is inherently challenging from experimental observations, because both processes exhibit a strong temperature and seasonal dependence. To constrain the role of oxidative processing, we examine molecular SOA tracers whose ratios are insensitive to emission strength in the PBL and instead reflect chemical aging under varying oxidative conditions.

Phthalic acid (PhA) and 4-methylphtalic acid (4-M-PhA) are both recognized as anthropogenic SOA tracers formed from aromatic precursor VOCs like *o*-xylene or naphthalene (Al-Naiema and Stone, 2017; Al-Naiema et al., 2020; Kleindienst et al., 2012). While benzene does not dominate the formation of PhA and 4-M-PhA as a precursor, it acts as a proxy for aromatic VOCs originating mostly from anthropogenic emission sources in the PBL, as its seasonal variability closely tracks that of other aromatics at the JFJ (Legreid et al., 2008). The ratio PhA/benzene and 4-M-PhA/benzene increase systematically with ω (Fig. 7a for PhA/Benzene, and Fig. S39 for 4-M-PhA/Benzene), by >4-fold across the observed ω-range, indicating enhanced SOA formation under elevated oxidative conditions. PBLi seems to play a subordinate role, based on the low dependence on NO_y/CO across the whole ω-range (cf. the comparable progression of binned local median trend lines in Fig. 7a).

Another independent evidence is provided on the basis of different biogenic α-pinene SOA markers. Pinic acid and pinonic acid are known early generation oxidation products, while 3-methyl-1,2,3-butanetricarboxylic acid (3-MBTCA) is a highly oxidized, late-generation product (Müller et al., 2012). As all three markers share the common precursor α-pinene, their ratios are decoupled from temperature-dependent biogenic VOC emission strengths. Pronounced shifts in molecular composition are observed both in absolute concentrations and relative abundances over the 11-year record (Fig. S40). Relative to pinic and pinonic acid, 3-MBTCA is strongly elevated during summer time while the former dominate in seasons closer to winter. The ratios 3-MBTCA/pinic acid and 3-MBTCA/pinonic acid increase strongly with ω (Fig. 7b and Fig. S41), by >5-fold, indicating enhanced chemical aging under elevated oxidative capacity. Especially at low ω, where the range of actinic flux is large, the dependence of 3-MBTCA/pinic acid on global radiation (color and binned local median trend lines in Fig. 7b) confirms that actinic flux can be an important predictor for OH production as well. However, under conditions characterized by high actinic

https://doi.org/10.5194/egusphere-2026-3660
Preprint. Discussion started: 7 July 2026

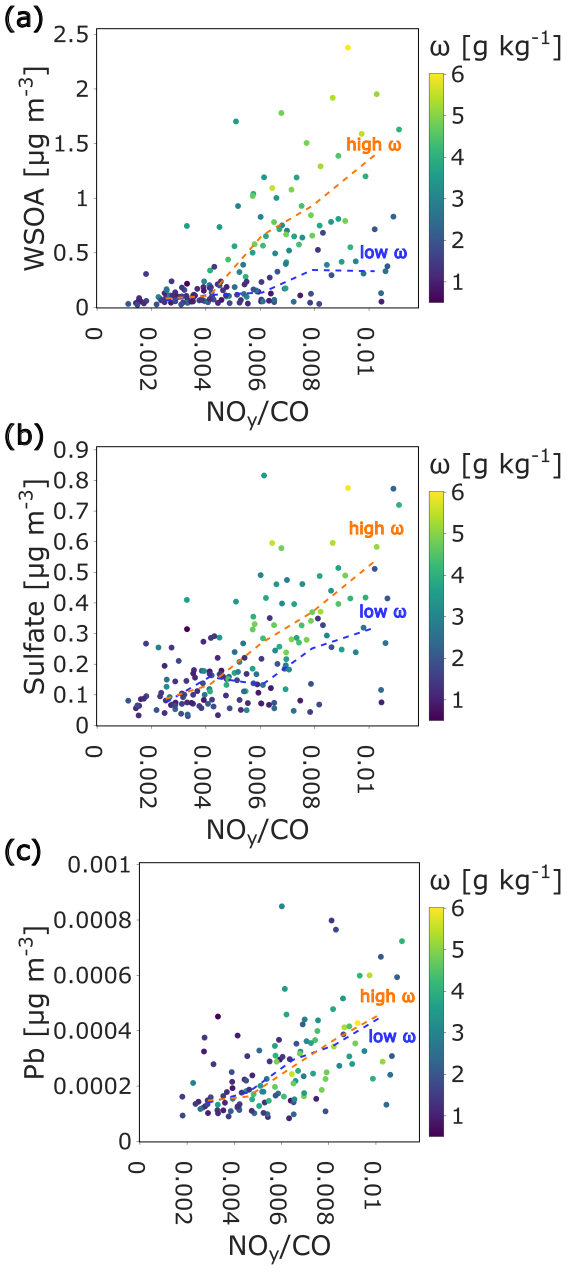

Figure 6. Mass concentrations of (a) WSOA, (b) sulfate and (c) Pb at the JFJ as a function of the PBLi tracer NO_y/CO, colored by the humidity ratio ω. Binned local median trend lines of mass concentrations vs. NO_y/CO for low (blue) and high (orange) ω are displayed. For this, data were stratified into five discrete NO_y/CO bins, locally segregated by upper/lower half of ω observations and the medians for the low and high ω groups were calculated to obtain trend lines. Sampling dates dominated by Saharan dust were omitted from all plots.

https://doi.org/10.5194/egusphere-2026-3660
Preprint. Discussion started: 7 July 2026

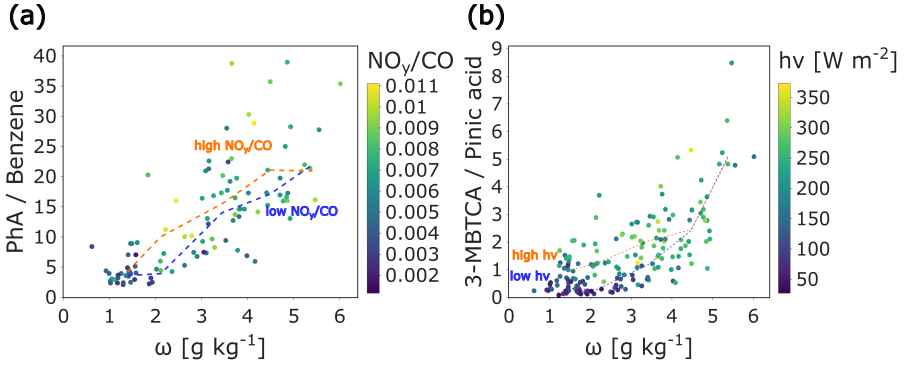

Figure 7. (a) Ratio of the anthropogenic SOA marker phthalic acid (PhA) mass concentration [$\mathrm{ng\,m^{-3}}$] and benzene mixing ratio [ppb] as a function of ω at the JFJ, colored by the PBLi tracer $\mathrm{NO_y/CO}$. (b) mass concentration [$\mathrm{ng\,m^{-3}}$] ratio of the biogenic SOA markers 3-MBTCA and pinic acid as a function of ω at the JFJ, colored by global radiation intensity ($h\nu$). Binned local median trend lines of the ratios vs. ω for low (blue) and high (orange) $\mathrm{NO_y/CO}$ or $h\nu$ are displayed. For this, data were stratified into six discrete ω bins, locally segregated by upper/lower half of $\mathrm{NO_y/CO}$ or $h\nu$ observations and the medians for the low and high $\mathrm{NO_y/CO}$ or $h\nu$ groups were calculated to obtain trend lines. Sampling dates dominated by Saharan dust were omitted from all plots.

flux variability, limited PBLi constrains precursor and water vapor supply, likely reducing the influence of actinic flux on secondary aerosol mass concentrations.

Together, these molecular constraints demonstrate that oxidative capacity exerts a first-order control on SOA formation and composition at the high-altitude receptor site. While precursor availability sets the potential for SOA formation, the extent of chemical aging — and thus the accumulation of highly oxidized products — is governed primarily by the oxidative history of the air mass, captured here by ω.

4.5 Contrasting molecular and bulk OA composition responses to oxidative processing and transport history

The observed behavior of SOA molecular markers — namely, enhanced aging under conditions of elevated atmospheric oxidative capacity — cannot be directly extrapolated to bulk OA properties and composition, as these additionally reflect variability in transport history and air-mass residence times. At the JFJ, FT-like conditions correspond to aged, PBL-decoupled air masses ($\geq$ 5 days), whereas PBLi conditions reflect diurnal vertical transport (Herrmann et al., 2015). To quantify how these regimes shape OA composition, WSOA was analyzed using complementary offline non-target mass spectrometric techniques and interpreted in the context of the proxies $\mathrm{NO_y/CO}$ (transport) and ω (oxidative capacity). For comparative analysis, the samples were categorized into three groups according to their corresponding $\mathrm{NO_y/CO}$ and ω levels. While only the water-soluble fraction is covered by this analysis, the very high water solubility of OA at the JFJ (median 83 % of OC, Sect. S10.3) assures a good representation also for the bulk OA.

The Offline-EESI-MS provides near-molecular resolution WSOA composition (Lopez-Hilfiker et al., 2019), with sensitivities strongly biased toward moderately oxidized compounds. For example, ions corresponding to the biogenic SOA species

https://doi.org/10.5194/egusphere-2026-3660
Preprint. Discussion started: 7 July 2026

3-MBTCA or 2-Methyltetrols exhibit Offline-EESI-MS signals orders of magnitude higher than the strongly aged oxalate, even though the latter dominates largely by mass (Sect. S3.4). A principal component analysis (PCA) of Offline-EESI-MS ion fractions (Fig. 8a) highlights clear differences in WSOA relative composition for the NO_y/CO-ω-categories. Chemical similarity is high for WSOA under low-ω conditions across the entire NO_y/CO-range, consistent with a dominance of FT residual aerosol even under strong PBLi (cf. the blue trend line in Fig. 6a). In contrast, the cluster associated with simultaneously high NO_y/CO and ω is well separated, indicating the impact of enhanced oxidative processing superimposed on strong biogenic emission intensities and PBLi. These conditions are associated with increased WSOA mass (cf. the orange trend line in Fig. 6a). On a molecular level, a systematic compositional shift toward more functionalized species is observed within the analyte range dominating Offline-EESI-MS (Fig. 8b), consistent with the molecular SOA markers (Sect. 4.4). This shift is characterized by a transition to lower carbon number compounds, with a dominance of C_8-C_{10} species likely representing oxidation products of monoterpenes, and an increase in oxygen content. Consistently, Offline-EESI-MS atomic O/C-ratios are systematically elevated with ω (Fig. S42).

Offline-AMS provides complementary insight into quantitative bulk WSOA composition, as it is analytically complete with respect to the WSOA mass (cf. the good agreement of Offline-AMS WSOA with TOC analyzer, considering OM/OC ratios derived from Offline-AMS, $SLR\ equation: WSOA_{AMS} = -0.16 + WSOA_{TOC} * 0.88$, $R^2 = 0.97$, Fig. S5). Similar to Offline-EESI-MS, the Offline-AMS PCA highlights the distinct WSOA composition at high-NO_y/CO-high-ω, indicated by a systematic difference from the low-ω conditions in PC1 (Fig. 9a). Accordingly, the median mass defect plot clearly differs from its low-ω counterparts (Fig. 9b). Two differences are particularly interesting: i) the fractions of CHN and CHON compounds are depleted under high-NO_y/CO-high-ω conditions, which could be related to a low availability of NO_x (Fig. 3a) and so nitrate radicals that are involved in formation of organonitrates (Ng et al., 2017); and ii) indifferent to PBLi, low-ω conditions exhibit elevated levels of ion fragments indicative of OA aging, such as CO^+ and CO_2^+, and depleted levels of the CH ion family. A moderately higher aging state at low-ω conditions is confirmed by elevated O/C- and decreased H/C-ratios derived from Offline-AMS (Fig. S43).

This might appear counterintuitive, given the role of ω as a proxy for the atmospheric oxidative capacity history and the pronounced aging observed at high ω for molecular SOA markers and Offline-EESI-MS. On a bulk OA level, however, the high oxidative age of comparably recently formed OA under PBLi-like conditions with strong OH exposure (high ω) is contrasted by the high atmospheric age ($\geq$ 5 days) of the FT residual OA dominating under all conditions with low ω. Although this substantial atmospheric age results in highly advanced OA aging, it is noteworthy that the elevated OH exposure characteristic to PBLi-dominated OA nearly offsets, in terms of chemical oxidation, a residence time difference of five days or more (O/C-ratios in Fig. S43). In consequence, bulk OA properties, such as O/C- and OM/OC-ratios (cf. Offline-AMS O/C timeseries in Fig. S44 and (Fröhlich et al., 2015)), show little seasonal variability at the JFJ despite different transport, formation and aging regimes governing the yearly OA cycles, which drive a distinct difference of molecular OA composition (as indicated by Offline-EESI-MS).

https://doi.org/10.5194/egusphere-2026-3660
Preprint. Discussion started: 7 July 2026

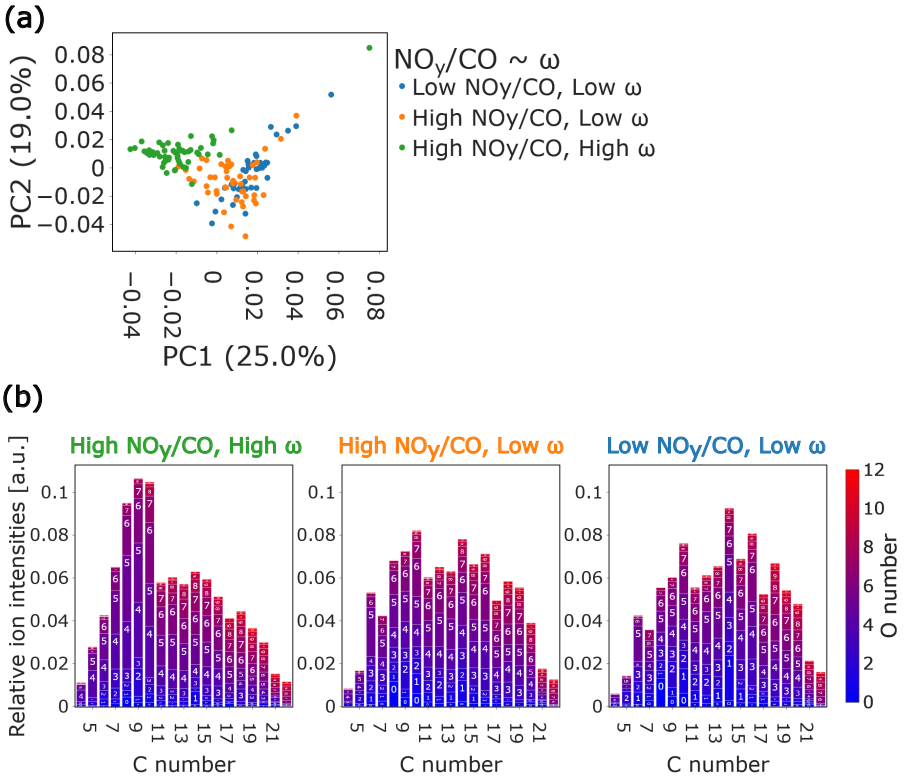

Figure 8. (a) Scatter plot of the first two PCA dimensions obtained from Offline-EESI-MS WSOA relative composition (ion signal fractions) at the JFJ. Data points are colored based on their categorization into NO_y/CO and ω groups, applying the following thresholds: '*Low* NO_y/CO' $\leq 0.004 <$ '*High* NO_y/CO' and '*Low* ω' $\leq 3\,g\,kg^{-1} <$ '*High* ω'. The explained variance of each PCA dimension is provided in parentheses. (b) For the corresponding NO_y/CO and ω groups, bar graphs of median relative EESI ion intensity fractions, stratified by carbon and oxygen numbers in the molecular formulas. Data is from composite filter samples from 2011 to 2019 and sampling dates dominated by Saharan dust were excluded.

5 Broader implications

The FT remains one of the least constrained regions of the atmosphere, despite exerting a disproportionate influence on aerosol–climate interactions. Global aerosol model intercomparison studies have long identified that limited observational coverage and an incomplete understanding of aerosol transport, secondary aerosol formation and physicochemical processing are main sources of the large uncertainties in simulated aerosol burdens in remote regions, particularly the FT (Tsigaridis et al., 2014; Hodzic et al., 2020). The 11-year record presented here provides a rare process-resolved view of aerosol evolution at the interface between the PBL and the FT. By leveraging the unique setting of the Jungfraujoch and the comprehensive chemical characterization over more than a decade, we directly track the formation and transformation of secondary (organic) aerosol during atmospheric transport, isolating the governing processes.

https://doi.org/10.5194/egusphere-2026-3660
Preprint. Discussion started: 7 July 2026

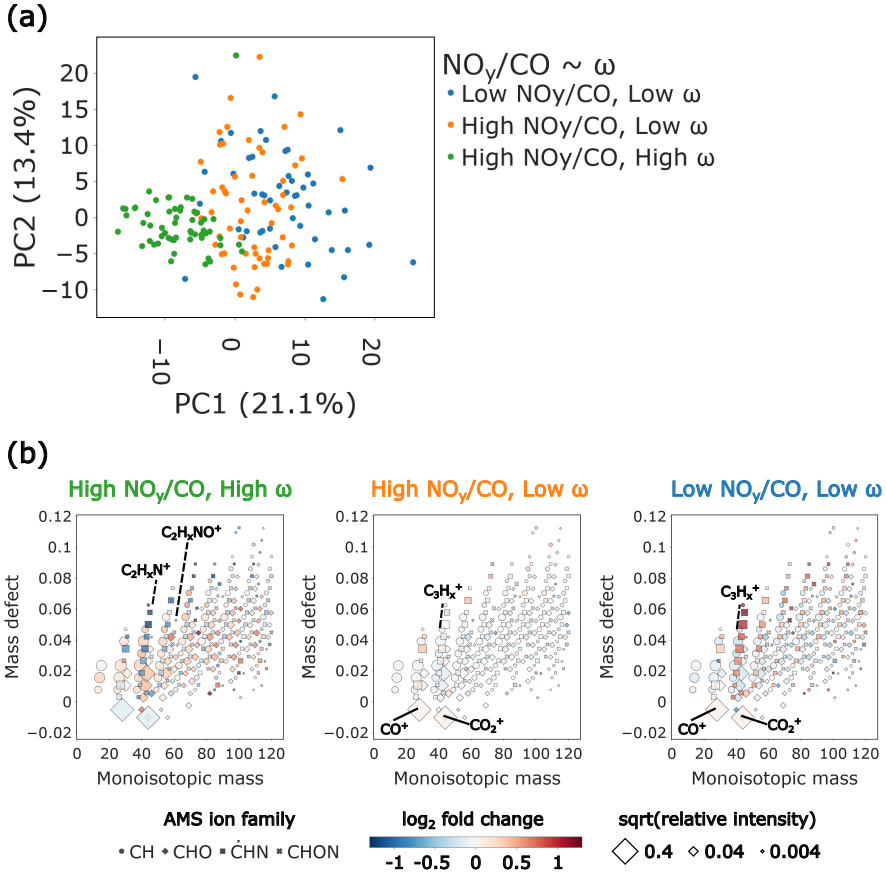

Figure 9. (a) Scatter plot of the first two PCA dimensions obtained from Offline-AMS relative WSOA composition (ion signal fractions) at the JFJ. Data points are colored based on their categorization into NO_y/CO and ω groups, applying the following thresholds: '*Low* NO_y/CO' $\leq 0.004 <$ '*High* NO_y/CO' and '*Low* ω' $\leq 3\,g\,kg^{-1} <$ '*High* ω'. The explained variance of each PCA dimension is provided in parentheses. (b) For the corresponding NO_y/CO and ω groups, mass defect plots of median Offline-AMS ion fractions. Marker symbols are selected based on ion families, sizes are based on the square root of their ion fraction contribution and colors correspond to the log_2 fold relative intensity change between the NO_y/CO and ω groups. Sampling dates dominated by Saharan dust were excluded.

A central result emerges with clarity: the atmospheric oxidative capacity experienced by PBLi air masses transported to high altitude is a primary driver of the observed secondary aerosol. The humidity ratio ω, commonly interpreted as a tracer of boundary layer influence, is shown here to capture the integrated oxidative history of air masses prior to arrival at the JFJ. While the role of water vapor in controlling ozone production is well established, our results demonstrate that it also exerts first-order control on secondary aerosol formation and chemical evolution. This finding provides an observational constraint on a key, yet poorly quantified, coupling between atmospheric composition, hydrological cycle, photochemistry, and aerosol formation.

https://doi.org/10.5194/egusphere-2026-3660
Preprint. Discussion started: 7 July 2026

This framework has immediate implications for a changing climate. A warmer and more humid atmosphere will, all else equal, enhance oxidative capacity through increased water vapor and sustained photochemical activity. Our observations suggest that such conditions will favor more efficient secondary aerosol formation and more rapid chemical aging during transport. At the same time, ongoing reductions in NO_x emissions will shift atmospheric chemistry toward lower-NO_x regimes, analogous to those observed at high altitude, promoting the formation of highly oxygenated OA and suppressing organonitrate pathways.

The proxies employed in this study — NO_y/CO for PBLi strength and ω for the atmospheric oxidative capacity — yield quantitative, observation-based constraints on relevant atmospheric processes. Such constraints are fundamental for advancing process-level understanding and for informing the optimization of atmospheric models. At the same time, important limitations remain. The strong co-variation of ω with temperature and season precludes a strict separation between oxidative processing and emission-driven effects for OA. Disentangling these contributions will require observations that simultaneously constrain precursor fluxes, oxidant concentrations, and chemical pathways, along with model validation.

The extent to which these findings translate to the polluted PBL is less straightforward. There, higher precursor concentrations and shorter timescales complicate the relationship between transport, oxidation, and aerosol formation. In this regard, the JFJ provides a unique natural laboratory, where the effects of atmospheric aging can be observed over extended timescales and under reduced interference from fresh emissions. As anthropogenic emissions decline and atmospheric composition evolves, PBL conditions may increasingly resemble those currently observed in the FT, suggesting that the processes identified here will become more broadly relevant.

Ultimately, these results underscore that aerosol properties at high altitude — and by extension their climatic effects — are not solely determined by emissions, but by the integrated history of transport and chemical processing. A more accurate representation of this interplay controlling aerosol concentrations and variability in the FT (especially the OA fraction) would benefit not only climate models. It would also considerably enhance our understanding of global biogeochemical transport cycles (Hobbs, 2000), the connections between atmospheric aerosols and high-altitude ice-core records (Baltensperger et al., 1991; Moseid et al., 2022), and the behavior and climate feedbacks of aerosols under changing climate conditions (Thornhill et al., 2021).

Code and data availability. The complete dataset used to generate the main text figures is openly accessible on Zenodo:

- Weng, J., El Haddad, I., Winiger, P., Reimann, S., Steinbacher, M., Brem, B. T., Gysel-Beer, M.: Online in-situ atmospheric data for: A Decadal-Scale Perspective on PM10 Composition and its Variability Drivers at the Alpine High-Altitude Research Station Jungfraujoch [data set]. Zenodo. https://doi.org/10.5281/zenodo.19913705, 2026.
- Weng, J., El Haddad, I., Winiger, P., Gkraikou, T., Oikonomou, K., Sciare, J., Ginot, P., Uzu, G., Jaffrezo, J.-L., Darfeuil, S.: Targeted mass spectrometry atmospheric data for: A Decadal-Scale Perspective on PM10 Composition and its Variability Drivers at the Alpine High-Altitude Research Station Jungfraujoch [data set]. Zenodo. https://doi.org/10.5281/zenodo.19918924, 2026.

https://doi.org/10.5194/egusphere-2026-3660
Preprint. Discussion started: 7 July 2026

– Weng, J., Hao, Y., El Haddad, I., Winiger, P.: Non-target mass spectrometry atmospheric water-soluble organic aerosol composition data for: A Decadal-Scale Perspective on PM10 Composition and its Variability Drivers at the Alpine High-Altitude Research Station Jungfraujoch [data set]. Zenodo. https://doi.org/10.5281/zenodo.20383919, 2026.

Part of the high-time-resolution online *in-situ* data has been archived before: aerosol absorption coefficient (2015 to 2021) — https://doi.org/10.48597/JP5A-632K; particle number size distribution (2020 to 2021) — https://doi.org/10.48597/B9EA-8B5B.

The code used for data processing and visualization is publicly available at GitHub and Zenodo (the exact versions used in this study are archived on Zenodo):

– Weng, J., Hao, Y., Winiger, P., El Haddad, I., Daellenbach, K. R.: Offline Aerosol Mass Spectrometry data analysis pipeline, https://github.com/wengjul/offline-ams-pipeline.git, and archived on Zenodo, https://doi.org/10.5281/zenodo.20528255, 2026.

– Weng, J., Hao, Y., Winiger, P., El Haddad, I., Daellenbach, K. R.: Offline Extractive Electrospray Ionization Mass Spectrometry data analysis pipeline, https://github.com/wengjul/offline-eesi-pipeline.git, and archived on Zenodo, https://doi.org/10.5281/zenodo.20542289, 2026.

– Weng, J., El Haddad, I., Winiger, P.: PM10 Composition and its Variability Drivers at the Jungfraujoch - Visualization code, https://github.com/wengjul/PM10-composition-JFJ.git, and archived on Zenodo, https://doi.org/10.5281/zenodo.20553692, 2026.

Code used for analysis and pre-processing of measurement data other than non-target mass spectrometry is available upon request.

Author contributions. According to CRediT taxonomy; **Julian Weng:** Conceptualization, Data curation, Formal analysis, Investigation, Methodology, Project administration, Software, Validation, Visualization, Writing (original draft preparation), Writing (review and editing). **Yufang Hao:** Investigation, Methodology, Software, Writing (review and editing). **Benjamin T. Brem:** Data curation, Investigation, Writing (review and editing). **Tianqu Cui:** Investigation, Methodology, Writing (review and editing). **Peeyush Khare:** Investigation, Methodology, Writing (review and editing). **Lubna Dada:** Formal analysis, Writing (review and editing). **Kaspar R. Daellenbach:** Methodology, Writing (review and editing). **Sophie Darfeuil:** Investigation, Data curation, Writing (review and editing). **Gaëlle Uzu:** Supervision, Writing (review and editing). **Jean-Luc Jaffrezo:** Supervision, Writing (review and editing). **Martin Steinbacher:** Investigation, Data curation, Writing (review and editing). **Stefan Reimann:** Investigation, Data curation, Writing (review and editing). **Thaleia Gkraikou:** Investigation, Writing (review and editing). **Konstantina Oikonomou:** Investigation, Writing (review and editing). **Jean Sciare:** Supervision, Writing (review and editing). **Martine Collaud Coen:** Data curation, Writing (review and editing). **Claudia Mohr:** Supervision, Writing (review and editing). **André S. H. Prévôt:** Supervision, Writing (review and editing). **Martin Gysel-Beer:** Data curation, Investigation, Project administration, Writing (review and editing). **Imad El Haddad:** Conceptualization, Funding acquisition, Investigation, Project administration, Supervision, Writing (review and editing). **Patrik Winiger:** Conceptualization, Funding acquisition, Investigation, Project administration, Supervision, Writing (review and editing).

Competing interests. The authors declare that they have no conflict of interest. Part of the funding was provided via a WeMakeIt Science-Booster crowdfunding campaign, including contributions from Digitel AG and Camfil GmbH. The funders had no involvement in the study design, data collection, analysis, interpretation, or manuscript preparation.

https://doi.org/10.5194/egusphere-2026-3660
Preprint. Discussion started: 7 July 2026

Acknowledgements. Xenia Kipouros is thanked for supporting filter water extraction procedures at PSI. Jens Top, Mihnea Surdu, Rico K. Y. Cheung and David Bell are thanked for instrumental support at PSI. Robin Lewis Modini, Nora Nowak, Leila Héloise Simon and Jay Slowik are thanked for discussions.

Christoph Hüglin from Empa is thanked for coordination of the NABEL network and assistance in the provision of the HiVol filters.

The authors wish to thank Marie Labat Saint Vincent for punching and transporting PM_{10} samples to Grenoble, and the AirOSol and PANDA analytical platforms at IGE (Institute of Environmental Geosciences, Grenoble, France) for providing laboratory facilities and technical support for the analysis of PM_{10} filters with UHPLC-MS/MS (Tristan Rousseau, Pauline Bros), IC-MS (Patrick Ginot, Isaure Landeche, Rhabira Elazzouzi and Zoia Poloubinski) and ICP-MS/MS (Clarisse Granon and Antoine Boyer) devices.

The $^{222}\mathrm{Rn}$ data were received from Franz Conen, University of Basel. He is grateful to Alastair Williams and his group at Australian Nuclear Science and Technology Organisation (ANSTO) for the ongoing collaboration as the supplier and supporter of the $^{222}\mathrm{Rn}$ detection system.

We would like to thank the International Foundation High Altitude Research Stations Jungfraujoch and Gornergrat (HFSJG), 3012 Bern, Switzerland, for enabling us to carry out our experiments at the Jungfraujoch High Altitude Research Station. We also thank the custodians Daniela Bissig and Erich Furrer, Sonja Stöckli and Thomas Furter, Christine and Ruedi Käser, Joan and Martin Fischer, Maria and Urs Otz, Susanne and Felix Seiler for the support of our activities, particularly the daily sampling of HiVol filters over a period of more than one decade. We thank Claudia Zellweger-Faesi, Nicole Bruggisser and David Steger from Empa for supporting the filter collection.

Financial support.

This work received funding support from the Swiss National Science Foundation (SNSF, project numbers: 200021_213071, PZ00P2_202178 and 216181) and from the Swiss Federal Office for the Environment, with further support from a WeMakeIt ScienceBooster crowdfunding, including contributions from Digitel AG and Camfil GmbH.

The continuous online-*in-situ* aerosol measurements at the JFJ receive financial support from MeteoSwiss in the framework of the Swiss contribution (GAW-CH) to the Global Atmosphere Watch program of the World Meteorological Organization (WMO), and from the Swiss State Secretariat for Education, Research and Innovation (SERI) in the framework of the Swiss contribution ACTRIS-CH to the ACTRIS ERIC. Measurements conducted by Empa are part of the Swiss National Air Pollution Monitoring Network which is jointly run by Empa and the Swiss Federal Office for the Environment (FOEN). VOC and NOx measurements are additionally supported through ACTRIS-CH and of CLIMGAS-CH.

The $^{222}\mathrm{Rn}$ observations are supported by the Swiss National Science Foundation (SNSF) as a contribution to the pan-European Integrated Carbon Observation System (ICOS) (grant 20FI-0_229655).

The AirOSol and PANDA analytical platforms at IGE were supported by different fundings: the IC-MS and ICP-MS/MS were funded through a donation from Thermo Fisher to the UGA Foundation as part of the Ice Memory program; the Sciex QTRAP 5500 LC-MS/MS was funded by a grant from Labex OSUG@2020 (investissements d'avenir ANR10-LABX56); the ANR program Atmospheric Biogenic Sugar ANR-21-CE01-0021-01 and the LEFE CHAT program with PMOA project (Organic Acids in Atmospheric PM, AO 2022) provided financial support for method development and part of JFJ PM_{10} analysis.

https://doi.org/10.5194/egusphere-2026-3660
Preprint. Discussion started: 7 July 2026

References

Al-Naiema, I. M. and Stone, E. A.: Evaluation of anthropogenic secondary organic aerosol tracers from aromatic hydrocarbons, Atmospheric Chemistry and Physics, 17, 2053–2065, https://doi.org/10.5194/acp-17-2053-2017, 2017.

Al-Naiema, I. M., Offenberg, J. H., Madler, C. J., Lewandowski, M., Kettler, J., Fang, T., and Stone, E. A.: Secondary organic aerosols from aromatic hydrocarbons and their contribution to fine particulate matter in Atlanta, Georgia, Atmospheric Environment, 223, 117 227, https://doi.org/10.1016/j.atmosenv.2019.117227, 2020.

Allen, A. G., Nemitz, E., Shi, J. P., Harrison, R. M., and Greenwood, J. C.: Size distributions of trace metals in atmospheric aerosols in the United Kingdom, Atmospheric Environment, 35, 4581–4591, https://doi.org/10.1016/S1352-2310(01)00190-X, 2001.

Ambrose, J. L., Reidmiller, D. R., and Jaffe, D. A.: Causes of high O3 in the lower free troposphere over the Pacific Northwest as observed at the Mt. Bachelor Observatory, Atmospheric Environment, 45, 5302–5315, https://doi.org/10.1016/j.atmosenv.2011.06.056, 2011.

Baltensperger, U., Gäggeler, H. W., Jost, D. T., Emmenegger, M., and Nägeli, W.: Continuous background aerosol monitoring with the epiphaniometer, Atmospheric Environment. Part A. General Topics, 25, 629–634, https://doi.org/10.1016/0960-1686(91)90060-K, 1991.

Baltensperger, U., Gäggeler, H. W., Jost, D. T., Lugauer, M., Schwikowski, M., Weingartner, E., and Seibert, P.: Aerosol climatology at the high-alpine site Jungfraujoch, Switzerland, Journal of Geophysical Research: Atmospheres, 102, 19 707–19 715, https://doi.org/10.1029/97JD00928, 1997.

Bond, T. C., Doherty, S. J., Fahey, D. W., Forster, P. M., Berntsen, T., DeAngelo, B. J., Flanner, M. G., Ghan, S., Kärcher, B., Koch, D., Kinne, S., Kondo, Y., Quinn, P. K., Sarofim, M. C., Schultz, M. G., Schulz, M., Venkataraman, C., Zhang, H., Zhang, S., Bellouin, N., Guttikunda, S. K., Hopke, P. K., Jacobson, M. Z., Kaiser, J. W., Klimont, Z., Lohmann, U., Schwarz, J. P., Shindell, D., Storelvmo, T., Warren, S. G., and Zender, C. S.: Bounding the role of black carbon in the climate system: A scientific assessment, Journal of Geophysical Research: Atmospheres, 118, 5380–5552, https://doi.org/10.1002/jgrd.50171, 2013.

Bros, P., Darfeuil, S., Jacob, V., Elazzouzi, R., Tusha, D., Rousseau, T., Weng, J., Winiger, P., El Haddad, I., Hueglin, C., Uzu, G., and Jaffrezo, J.-L.: Quantification of 21 sugars in tropospheric particulate matter by ultra-high-performance liquid chromatography tandem mass spectrometry, Atmospheric Measurement Techniques, 18, 6315–6327, https://doi.org/10.5194/amt-18-6315-2025, 2025.

Buck, A. L.: New Equations for Computing Vapor Pressure and Enhancement Factor, Journal of Applied Meteorology and Climatology, 20, 1527–1532, https://doi.org/10.1175/1520-0450(1981)020<1527:NEFCVP>2.0.CO;2, 1981.

Bukowiecki, N., Weingartner, E., Gysel, M., Coen, M. C., Zieger, P., Herrmann, E., Steinbacher, M., Gäggeler, H. W., and Baltensperger, U.: A Review of More than 20 Years of Aerosol Observation at the High Altitude Research Station Jungfraujoch, Switzerland (3580 m asl), Aerosol and Air Quality Research, 16, 764–788, https://doi.org/10.4209/aaqr.2015.05.0305, 2016.

Cavalli, F., Viana, M., Yttri, K. E., Genberg, J., and Putaud, J.-P.: Toward a standardised thermal-optical protocol for measuring atmospheric organic and elemental carbon: the EUSAAR protocol, Atmospheric Measurement Techniques, 3, 79–89, https://doi.org/10.5194/amt-3-79-2010, 2010.

Chow, J. C., Watson, J. G., Lowenthal, D. H., and Magliano, K. L.: Loss of $PM_{2.5}$ Nitrate from Filter Samples in Central California, Journal of the Air & Waste Management Association, 55, 1158–1168, https://doi.org/10.1080/10473289.2005.10464704, 2005.

Collaud Coen, M., Weingartner, E., Schaub, D., Hueglin, C., Corrigan, C., Henning, S., Schwikowski, M., and Baltensperger, U.: Saharan dust events at the Jungfraujoch: detection by wavelength dependence of the single scattering albedo and first climatology analysis, Atmospheric Chemistry and Physics, 4, 2465–2480, https://doi.org/10.5194/acp-4-2465-2004, 2004.

https://doi.org/10.5194/egusphere-2026-3660
Preprint. Discussion started: 7 July 2026

Collaud Coen, M., Weingartner, E., Nyeki, S., Cozic, J., Henning, S., Verheggen, B., Gehrig, R., and Baltensperger, U.: Long-term trend analysis of aerosol variables at the high-alpine site Jungfraujoch, Journal of Geophysical Research: Atmospheres, 112, https://doi.org/10.1029/2006JD007995, 2007.

Collaud Coen, M., Weingartner, E., Furger, M., Nyeki, S., Prévôt, A. S. H., Steinbacher, M., and Baltensperger, U.: Aerosol climatology and planetary boundary influence at the Jungfraujoch analyzed by synoptic weather types, Atmospheric Chemistry and Physics, 11, 5931–5944, https://doi.org/10.5194/acp-11-5931-2011, 2011.

Collaud Coen, M., Andrews, E., Aliaga, D., Andrade, M., Angelov, H., Bukowiecki, N., Ealo, M., Fialho, P., Flentje, H., Hallar, A. G., Hooda, R., Kalapov, I., Krejci, R., Lin, N.-H., Marinoni, A., Ming, J., Nguyen, N. A., Pandolfi, M., Pont, V., Ries, L., Rodríguez, S., Schauer, G., Sellegri, K., Sharma, S., Sun, J., Tunved, P., Velasquez, P., and Ruffieux, D.: Identification of topographic features influencing aerosol observations at high altitude stations, Atmospheric Chemistry and Physics, 18, 12 289–12 313, https://doi.org/10.5194/acp-18-12289-2018, 2018.

Collaud Coen, M., Brem, B. T., Gysel-Beer, M., Modini, R., Henne, S., Steinbacher, M., Putero, D., Gini, M. I., and Eleftheriadis, K.: Detection and climatology of Saharan dust frequency and mass at the Jungfraujoch (3580 m a.s.l., Switzerland), Atmospheric Chemistry and Physics, 26, 1623–1645, https://doi.org/10.5194/acp-26-1623-2026, 2026.

Cozic, J., Verheggen, B., Weingartner, E., Crosier, J., Bower, K. N., Flynn, M., Coe, H., Henning, S., Steinbacher, M., Henne, S., Collaud Coen, M., Petzold, A., and Baltensperger, U.: Chemical composition of free tropospheric aerosol for PM1 and coarse mode at the high alpine site Jungfraujoch, Atmospheric Chemistry and Physics, 8, 407–423, https://doi.org/10.5194/acp-8-407-2008, 2008.

Croft, B., Pierce, J. R., and Martin, R. V.: Interpreting aerosol lifetimes using the GEOS-Chem model and constraints from radionuclide measurements, Atmospheric Chemistry and Physics, 14, 4313–4325, https://doi.org/10.5194/acp-14-4313-2014, 2014.

Cui, T., Manousakas, M. I., Wang, Q., Uzu, G., Hao, Y., Khare, P., Qi, L., Chen, Y., Han, Y., Slowik, J. G., Jaffrezo, J.-L., Cao, J., Prévôt, A. S. H., and Daellenbach, K. R.: Composition and Sources of Organic Aerosol in Two Megacities in Western China Using Complementary Mass Spectrometric and Statistical Techniques, ACS ES&T Air, 1, 1053–1065, https://doi.org/10.1021/acsestair.4c00051, 2024.

Daellenbach, K. R., Bozzetti, C., Křepelová, A., Canonaco, F., Wolf, R., Zotter, P., Fermo, P., Crippa, M., Slowik, J. G., Sosedova, Y., Zhang, Y., Huang, R.-J., Poulain, L., Szidat, S., Baltensperger, U., El Haddad, I., and Prévôt, A. S. H.: Characterization and source apportionment of organic aerosol using offline aerosol mass spectrometry, Atmospheric Measurement Techniques, 9, 23–39, https://doi.org/10.5194/amt-9-23-2016, 2016.

European Environment Agency: Europe's air quality status 2021, EEA report (Online), Publications Office, LU, https://doi.org/10.2800/488115, 2022.

Fröhlich, R., Cubison, M. J., Slowik, J. G., Bukowiecki, N., Canonaco, F., Croteau, P. L., Gysel, M., Henne, S., Herrmann, E., Jayne, J. T., Steinbacher, M., Worsnop, D. R., Baltensperger, U., and Prévôt, A. S. H.: Fourteen months of on-line measurements of the non-refractory submicron aerosol at the Jungfraujoch (3580 m a.s.l.) – chemical composition, origins and organic aerosol sources, Atmospheric Chemistry and Physics, 15, 11 373–11 398, https://doi.org/10.5194/acp-15-11373-2015, 2015.

Griffiths, A. D., Conen, F., Weingartner, E., Zimmermann, L., Chambers, S. D., Williams, A. G., and Steinbacher, M.: Surface-to-mountaintop transport characterised by radon observations at the Jungfraujoch, Atmospheric Chemistry and Physics, 14, 12 763–12 779, https://doi.org/10.5194/acp-14-12763-2014, 2014.

Hao, Y., Strähl, J., Khare, P., Cui, T., Schneider-Beltran, K., Qi, L., Wang, D., Top, J., Surdu, M., Bhattu, D., Bhowmik, H. S., Vats, P., Rai, P., Kumar, V., Ganguly, D., Szidat, S., Uzu, G., Jaffrezo, J.-L., Elazzouzi, R., Rastogi, N., Slowik, J., Haddad, I. E., Tripathi, S. N., Prévôt,

https://doi.org/10.5194/egusphere-2026-3660
Preprint. Discussion started: 7 July 2026

A. S. H., and Daellenbach, K. R.: Transported smoke from crop residue burning as the major source of organic aerosol and health risks in northern Indian cities during post-monsoon, Environment International, 202, 109 583, https://doi.org/10.1016/j.envint.2025.109583, 2025.

Heald, C. L., Coe, H., Jimenez, J. L., Weber, R. J., Bahreini, R., Middlebrook, A. M., Russell, L. M., Jolleys, M., Fu, T.-M., Allan, J. D., Bower, K. N., Capes, G., Crosier, J., Morgan, W. T., Robinson, N. H., Williams, P. I., Cubison, M. J., DeCarlo, P. F., and Dunlea, E. J.: Exploring the vertical profile of atmospheric organic aerosol: comparing 17 aircraft field campaigns with a global model, Atmospheric Chemistry and Physics, 11, 12 673–12 696, https://doi.org/10.5194/acp-11-12673-2011, 2011.

Henne, S., Furger, M., Nyeki, S., Steinbacher, M., Neininger, B., de Wekker, S. F. J., Dommen, J., Spichtinger, N., Stohl, A., and Prévôt, A. S. H.: Quantification of topographic venting of boundary layer air to the free troposphere, Atmospheric Chemistry and Physics, 4, 497–509, https://doi.org/10.5194/acp-4-497-2004, 2004.

Henne, S., Furger, M., and Prévôt, A. H.: Climatology of Mountain Venting–Induced Elevated Moisture Layers in the Lee of the Alps, Journal of Applied Meteorology and Climatology, 44, 620–633, https://doi.org/10.1175/JAM2217.1, 2005.

Henne, S., Brunner, D., Folini, D., Solberg, S., Klausen, J., and Buchmann, B.: Assessment of parameters describing representativeness of air quality in-situ measurement sites, Atmospheric Chemistry and Physics, 10, 3561–3581, https://doi.org/10.5194/acp-10-3561-2010, 2010.

Herrmann, E., Weingartner, E., Henne, S., Vuilleumier, L., Bukowiecki, N., Steinbacher, M., Conen, F., Collaud Coen, M., Hammer, E., Jurányi, Z., Baltensperger, U., and Gysel, M.: Analysis of long-term aerosol size distribution data from Jungfraujoch with emphasis on free tropospheric conditions, cloud influence, and air mass transport, Journal of Geophysical Research: Atmospheres, 120, 9459–9480, https://doi.org/10.1002/2015JD023660, 2015.

Hobbs, P. V., ed.: Tropospheric chemical cycles, Cambridge University Press, Cambridge, ISBN 978-0-521-77800-8, https://doi.org/10.1017/CBO9780511808913.009, 2000.

Hodzic, A., Campuzano-Jost, P., Bian, H., Chin, M., Colarco, P. R., Day, D. A., Froyd, K. D., Heinold, B., Jo, D. S., Katich, J. M., Kodros, J. K., Nault, B. A., Pierce, J. R., Ray, E., Schacht, J., Schill, G. P., Schroder, J. C., Schwarz, J. P., Sueper, D. T., Tegen, I., Tilmes, S., Tsigaridis, K., Yu, P., and Jimenez, J. L.: Characterization of organic aerosol across the global remote troposphere: a comparison of ATom measurements and global chemistry models, Atmospheric Chemistry and Physics, 20, 4607–4635, https://doi.org/10.5194/acp-20-4607-2020, 2020.

Hueglin, C., Gehrig, R., Baltensperger, U., Gysel, M., Monn, C., and Vonmont, H.: Chemical characterisation of PM2.5, PM10 and coarse particles at urban, near-city and rural sites in Switzerland, Atmospheric Environment, 39, 637–651, https://doi.org/10.1016/j.atmosenv.2004.10.027, 2005.

Hueglin, C., Buchmann, B., Steinbacher, M., and Emmenegger, L.: The Swiss National Air Pollution Monitoring Network (NABEL) – Bridging Science and Environmental Policy, CHIMIA, 78, 722–727, https://doi.org/10.2533/chimia.2024.722, 2024.

Jimenez, J. L., Canagaratna, M. R., Donahue, N. M., Prevot, A. S. H., Zhang, Q., Kroll, J. H., DeCarlo, P. F., Allan, J. D., Coe, H., Ng, N. L., Aiken, A. C., Docherty, K. S., Ulbrich, I. M., Grieshop, A. P., Robinson, A. L., Duplissy, J., Smith, J. D., Wilson, K. R., Lanz, V. A., Hueglin, C., Sun, Y. L., Tian, J., Laaksonen, A., Raatikainen, T., Rautiainen, J., Vaattovaara, P., Ehn, M., Kulmala, M., Tomlinson, J. M., Collins, D. R., Cubison, M. J., E., Dunlea, J., Huffman, J. A., Onasch, T. B., Alfarra, M. R., Williams, P. I., Bower, K., Kondo, Y., Schneider, J., Drewnick, F., Borrmann, S., Weimer, S., Demerjian, K., Salcedo, D., Cottrell, L., Griffin, R., Takami, A., Miyoshi, T., Hatakeyama, S., Shimono, A., Sun, J. Y., Zhang, Y. M., Dzepina, K., Kimmel, J. R., Sueper, D., Jayne, J. T., Herndon, S. C., Trimborn, A. M., Williams, L. R., Wood, E. C., Middlebrook, A. M., Kolb, C. E., Baltensperger, U., and Worsnop, D. R.: Evolution of Organic Aerosols in the Atmosphere, Science, 326, 1525–1529, https://doi.org/10.1126/science.1180353, 2009.

https://doi.org/10.5194/egusphere-2026-3660
Preprint. Discussion started: 7 July 2026

Jin, X., Cai, X., Wang, X., Huang, Q., Song, Y., Kang, L., Zhang, H., and Zhu, T.: Water vapour exchange between the atmospheric boundary layer and free troposphere over eastern China: seasonal characteristics and the El Niño–Southern Oscillation anomaly, Atmospheric Chemistry and Physics, 24, 259–274, https://doi.org/10.5194/acp-24-259-2024, 2024.

Jurányi, Z., Gysel, M., Weingartner, E., Bukowiecki, N., Kammermann, L., and Baltensperger, U.: A 17 month climatology of the cloud condensation nuclei number concentration at the high alpine site Jungfraujoch, Journal of Geophysical Research: Atmospheres, 116, https://doi.org/10.1029/2010JD015199, 2011.

Kleindienst, T. E., Jaoui, M., Lewandowski, M., Offenberg, J. H., and Docherty, K. S.: The formation of SOA and chemical tracer compounds from the photooxidation of naphthalene and its methyl analogs in the presence and absence of nitrogen oxides, Atmospheric Chemistry and Physics, 12, 8711–8726, https://doi.org/10.5194/acp-12-8711-2012, 2012.

Kok, J. F., Storelvmo, T., Karydis, V. A., Adebiyi, A. A., Mahowald, N. M., Evan, A. T., He, C., and Leung, D. M.: Mineral dust aerosol impacts on global climate and climate change, Nature Reviews Earth & Environment, 4, 71–86, https://doi.org/10.1038/s43017-022-00379-5, 2023.

Legreid, G., Folini, D., Staehelin, J., Balzani Lööv, J., Steinbacher, M., and Reimann, S.: Measurements of organic trace gases including oxygenated volatile organic compounds at the high alpine site Jungfraujoch (Switzerland): Seasonal variation and source allocations, Journal of Geophysical Research: Atmospheres, 113, https://doi.org/10.1029/2007JD008653, 2008.

Lelieveld, J., Gromov, S., Pozzer, A., and Taraborrelli, D.: Global tropospheric hydroxyl distribution, budget and reactivity, Atmospheric Chemistry and Physics, 16, 12 477–12 493, https://doi.org/10.5194/acp-16-12477-2016, 2016.

Leuenberger, M. and Flückiger, E.: Research at Jungfraujoch, Science of The Total Environment, 391, 169–176, https://doi.org/10.1016/j.scitotenv.2007.10.044, 2008.

Liu, Y., Dong, X., Wang, M., Emmons, L. K., Liu, Y., Liang, Y., Li, X., and Shrivastava, M.: Analysis of secondary organic aerosol simulation bias in the Community Earth System Model (CESM2.1), Atmospheric Chemistry and Physics, 21, 8003–8021, https://doi.org/10.5194/acp-21-8003-2021, 2021.

Lohmann, U. and Feichter, J.: Global indirect aerosol effects: a review, Atmospheric Chemistry and Physics, 5, 715–737, https://doi.org/10.5194/acp-5-715-2005, 2005.

Lopez-Hilfiker, F. D., Pospisilova, V., Huang, W., Kalberer, M., Mohr, C., Stefenelli, G., Thornton, J. A., Baltensperger, U., Prevot, A. S. H., and Slowik, J. G.: An extractive electrospray ionization time-of-flight mass spectrometer (EESI-TOF) for online measurement of atmospheric aerosol particles, Atmospheric Measurement Techniques, 12, 4867–4886, https://doi.org/10.5194/amt-12-4867-2019, 2019.

Moreno, C. I., Krejci, R., Jaffrezo, J.-L., Uzu, G., Alastuey, A., Andrade, M. F., Mardóñez, V., Koenig, A. M., Aliaga, D., Mohr, C., Ticona, L., Velarde, F., Blacutt, L., Forno, R., Whiteman, D. N., Wiedensohler, A., Ginot, P., and Laj, P.: Tropical tropospheric aerosol sources and chemical composition observed at high altitude in the Bolivian Andes, Atmospheric Chemistry and Physics, 24, 2837–2860, https://doi.org/10.5194/acp-24-2837-2024, 2024.

Moseid, K. O., Schulz, M., Eichler, A., Schwikowski, M., McConnell, J. R., Olivié, D., Criscitiello, A. S., Kreutz, K. J., and Legrand, M.: Using Ice Cores to Evaluate CMIP6 Aerosol Concentrations Over the Historical Era, Journal of Geophysical Research: Atmospheres, 127, e2021JD036 105, https://doi.org/10.1029/2021JD036105, 2022.

Myhre, G., Samset, B. H., Schulz, M., Balkanski, Y., Bauer, S., Berntsen, T. K., Bian, H., Bellouin, N., Chin, M., Diehl, T., Easter, R. C., Feichter, J., Ghan, S. J., Hauglustaine, D., Iversen, T., Kinne, S., Kirkevåg, A., Lamarque, J.-F., Lin, G., Liu, X., Lund, M. T., Luo, G., Ma, X., van Noije, T., Penner, J. E., Rasch, P. J., Ruiz, A., Seland, , Skeie, R. B., Stier, P., Takemura, T., Tsigaridis, K., Wang, P., Wang,

https://doi.org/10.5194/egusphere-2026-3660
Preprint. Discussion started: 7 July 2026

Z., Xu, L., Yu, H., Yu, F., Yoon, J.-H., Zhang, K., Zhang, H., and Zhou, C.: Radiative forcing of the direct aerosol effect from AeroCom Phase II simulations, Atmospheric Chemistry and Physics, 13, 1853–1877, https://doi.org/10.5194/acp-13-1853-2013, 2013.

Müller, L., Reinnig, M.-C., Naumann, K. H., Saathoff, H., Mentel, T. F., Donahue, N. M., and Hoffmann, T.: Formation of 3-methyl-1,2,3-butanetricarboxylic acid via gas phase oxidation of pinonic acid – a mass spectrometric study of SOA aging, Atmospheric Chemistry and Physics, 12, 1483–1496, https://doi.org/10.5194/acp-12-1483-2012, 2012.

Ng, N. L., Brown, S. S., Archibald, A. T., Atlas, E., Cohen, R. C., Crowley, J. N., Day, D. A., Donahue, N. M., Fry, J. L., Fuchs, H., Griffin, R. J., Guzman, M. I., Herrmann, H., Hodzic, A., Iinuma, Y., Jimenez, J. L., Kiendler-Scharr, A., Lee, B. H., Luecken, D. J., Mao, J., McLaren, R., Mutzel, A., Osthoff, H. D., Ouyang, B., Picquet-Varrault, B., Platt, U., Pye, H. O. T., Rudich, Y., Schwantes, R. H., Shiraiwa, M., Stutz, J., Thornton, J. A., Tilgner, A., Williams, B. J., and Zaveri, R. A.: Nitrate radicals and biogenic volatile organic compounds: oxidation, mechanisms, and organic aerosol, Atmospheric Chemistry and Physics, 17, 2103–2162, https://doi.org/10.5194/acp-17-2103-2017, 2017.

O'Brien, R. J., Green, P. J., and Doty, R. A.: Rate constant for the reaction NO2 + OH + M -> HNO3 + M measured under simulated atmospheric conditions using a novel analysis procedure, The Journal of Physical Chemistry, 83, 3302–3305, https://doi.org/10.1021/j100488a024, 1979.

Obrist, D., Hallar, A. G., McCubbin, I., Stephens, B. B., and Rahn, T.: Atmospheric mercury concentrations at Storm Peak Laboratory in the Rocky Mountains: Evidence for long-range transport from Asia, boundary layer contributions, and plant mercury uptake, Atmospheric Environment, 42, 7579–7589, https://doi.org/10.1016/j.atmosenv.2008.06.051, 2008.

Okamoto, S. and Tanimoto, H.: A review of atmospheric chemistry observations at mountain sites, Progress in Earth and Planetary Science, 3, 34, https://doi.org/10.1186/s40645-016-0109-2, 2016.

Pai, S. J., Heald, C. L., Pierce, J. R., Farina, S. C., Marais, E. A., Jimenez, J. L., Campuzano-Jost, P., Nault, B. A., Middlebrook, A. M., Coe, H., Shilling, J. E., Bahreini, R., Dingle, J. H., and Vu, K.: An evaluation of global organic aerosol schemes using airborne observations, Atmospheric Chemistry and Physics, 20, 2637–2665, https://doi.org/10.5194/acp-20-2637-2020, 2020.

Price, P., Bottorff, B., Jenkins, J., Brune, W. H., and Stevens, P. S.: Re-assessing hydroxyl radical chemistry in the atmosphere: Instrument interferences may explain previous measurement discrepancies, Communications Earth & Environment, 6, 325, https://doi.org/10.1038/s43247-025-02308-y, 2025.

Putaud, J.-P., Cavalli, F., Yttri, K. E., Chow, J. C., Watson, J. G., Sinha, B., Venkataraman, C., Ikemori, F., Jaffrezo, J.-L., Uzu, G., Moreno, I., Krejci, R., Laj, P., Gupta, T., Hu, M., Kim, S.-W., Mayol-Bracero, O., Quinn, P., Aas, W., Alastuey, A., Andrade, M., Angelucci, M., Anurag, G., Beukes, J. P., Bhardwaj, A., Chatterjee, A., Chaudhary, P., Chhangani, A. K., Conil, S., Degorska, A., Devaliya, S., Dhandapani, A., Duhan, S. S., Chandra Dumka, U., Habib, G., Hamzavi, Z., Haswani, D., Herrmann, H., Holubova, A., Hueglin, C., Imran, M., Jehangir, A., Kapoor, T. S., Karanasiou, A., Khaiwal, R., Kim, J., Kolesa, T., Kozakiewicz, J., Kranjc, I., Laura, J. S., Lian, Y., Liu, J., Manwani, P., Mardoñez-Balderrama, V., Marticorena, B., Matsuki, A., Mor, S., Mukherjee, S., Murthy, S., Muthalagu, A., Najar, T. A., Kumar, R. N., Pandithurai, G., Perez, N., Phairuang, W., Phuleria, H. C., Poulain, L., Prasad, L., Pullokaran, D., Qadri, A. M., Qureshi, A., Ramírez, O., Roy, S., Rüdiger, J., Saikia, B. K., Saikia, P., Sauvage, S., Savvides, C., Sharma, R., Singh, T., Singh, G. K., Spoor, R., Srivastava, A. K., Raman, R. S., Van Zyl, P. G., Vecchiocattivi, M., Voiron, C., Xin, J., and Yadav, K.: A worldwide aerosol phenomenology: Elemental and organic carbon in PM2.5 and PM10, Atmospheric Environment, 358, 121 338, https://doi.org/10.1016/j.atmosenv.2025.121338, 2025.

https://doi.org/10.5194/egusphere-2026-3660
Preprint. Discussion started: 7 July 2026

Rohrer, F., Lu, K., Hofzumahaus, A., Bohn, B., Brauers, T., Chang, C.-C., Fuchs, H., Häseler, R., Holland, F., Hu, M., Kita, K., Kondo, Y., Li, X., Lou, S., Oebel, A., Shao, M., Zeng, L., Zhu, T., Zhang, Y., and Wahner, A.: Maximum efficiency in the hydroxyl-radical-based self-cleansing of the troposphere, Nature Geoscience, 7, 559–563, https://doi.org/10.1038/ngeo2199, 2014.

Samaké, A., Jaffrezo, J.-L., Favez, O., Weber, S., Jacob, V., Albinet, A., Riffault, V., Perdrix, E., Waked, A., Golly, B., Salameh, D., Chevrier, F., Oliveira, D. M., Bonnaire, N., Besombes, J.-L., Martins, J. M. F., Conil, S., Guillaud, G., Mesbah, B., Rocq, B., Robic, P.-Y., Hulin, A., Le Meur, S., Descheemaecker, M., Chretien, E., Marchand, N., and Uzu, G.: Polyols and glucose particulate species as tracers of primary biogenic organic aerosols at 28 French sites, Atmospheric Chemistry and Physics, 19, 3357–3374, https://doi.org/10.5194/acp-19-3357-2019, 2019.

Samset, B. H. and Myhre, G.: Vertical dependence of black carbon, sulphate and biomass burning aerosol radiative forcing, Geophysical Research Letters, 38, https://doi.org/10.1029/2011GL049697, 2011.

Schuepbach, E., Friedli, T. K., Zanis, P., Monks, P. S., and Penkett, S. A.: State space analysis of changing seasonal ozone cycles (1988–1997) at Jungfraujoch (3580 m above sea level) in Switzerland, Journal of Geophysical Research: Atmospheres, 106, 20 413–20 427, https://doi.org/10.1029/2000JD900591, 2001.

Shafer, M. M., Toner, B. M., Overdier, J. T., Schauer, J. J., Fakra, S. C., Hu, S., Herner, J. D., and Ayala, A.: Chemical Speciation of Vanadium in Particulate Matter Emitted from Diesel Vehicles and Urban Atmospheric Aerosols, Environmental Science & Technology, 46, 189–195, https://doi.org/10.1021/es200463c, 2012.

Sporre, M. K., Blichner, S. M., Karset, I. H. H., Makkonen, R., and Berntsen, T. K.: BVOC–aerosol–climate feedbacks investigated using NorESM, Atmospheric Chemistry and Physics, 19, 4763–4782, https://doi.org/10.5194/acp-19-4763-2019, 2019.

Spracklen, D. V., Jimenez, J. L., Carslaw, K. S., Worsnop, D. R., Evans, M. J., Mann, G. W., Zhang, Q., Canagaratna, M. R., Allan, J., Coe, H., McFiggans, G., Rap, A., and Forster, P.: Aerosol mass spectrometer constraint on the global secondary organic aerosol budget, Atmospheric Chemistry and Physics, 11, 12 109–12 136, https://doi.org/10.5194/acp-11-12109-2011, 2011.

Stone, D., Whalley, L. K., and Heard, D. E.: Tropospheric OH and HO2 radicals: field measurements and model comparisons, Chemical Society Reviews, 41, 6348–6404, https://doi.org/10.1039/C2CS35140D, 2012.

Textor, C., Schulz, M., Guibert, S., Kinne, S., Balkanski, Y., Bauer, S., Berntsen, T., Berglen, T., Boucher, O., Chin, M., Dentener, F., Diehl, T., Easter, R., Feichter, H., Fillmore, D., Ghan, S., Ginoux, P., Gong, S., Grini, A., Hendricks, J., Horowitz, L., Huang, P., Isaksen, I., Iversen, I., Kloster, S., Koch, D., Kirkevåg, A., Kristjansson, J. E., Krol, M., Lauer, A., Lamarque, J. F., Liu, X., Montanaro, V., Myhre, G., Penner, J., Pitari, G., Reddy, S., Seland, , Stier, P., Takemura, T., and Tie, X.: Analysis and quantification of the diversities of aerosol life cycles within AeroCom, Atmospheric Chemistry and Physics, 6, 1777–1813, https://doi.org/10.5194/acp-6-1777-2006, 2006.

Thornhill, G., Collins, W., Olivié, D., Skeie, R. B., Archibald, A., Bauer, S., Checa-Garcia, R., Fiedler, S., Folberth, G., Gjermundsen, A., Horowitz, L., Lamarque, J.-F., Michou, M., Mulcahy, J., Nabat, P., Naik, V., O'Connor, F. M., Paulot, F., Schulz, M., Scott, C. E., Séférian, R., Smith, C., Takemura, T., Tilmes, S., Tsigaridis, K., and Weber, J.: Climate-driven chemistry and aerosol feedbacks in CMIP6 Earth system models, Atmospheric Chemistry and Physics, 21, 1105–1126, https://doi.org/10.5194/acp-21-1105-2021, 2021.

Timonen, H., Jaffe, D. A., Wigder, N., Hee, J., Gao, H., Pitzman, L., and Cary, R. A.: Sources of carbonaceous aerosol in the free troposphere, Atmospheric Environment, 92, 146–153, https://doi.org/10.1016/j.atmosenv.2014.04.014, 2014.

Tsigaridis, K., Daskalakis, N., Kanakidou, M., Adams, P. J., Artaxo, P., Bahadur, R., Balkanski, Y., Bauer, S. E., Bellouin, N., Benedetti, A., Bergman, T., Berntsen, T. K., Beukes, J. P., Bian, H., Carslaw, K. S., Chin, M., Curci, G., Diehl, T., Easter, R. C., Ghan, S. J., Gong, S. L., Hodzic, A., Hoyle, C. R., Iversen, T., Jathar, S., Jimenez, J. L., Kaiser, J. W., Kirkevåg, A., Koch, D., Kokkola, H., Lee, Y. H., Lin, G., Liu, X., Luo, G., Ma, X., Mann, G. W., Mihalopoulos, N., Morcrette, J.-J., Müller, J.-F., Myhre, G., Myriokefalitakis, S., Ng, N. L.,

https://doi.org/10.5194/egusphere-2026-3660
Preprint. Discussion started: 7 July 2026

O'Donnell, D., Penner, J. E., Pozzoli, L., Pringle, K. J., Russell, L. M., Schulz, M., Sciare, J., Seland, , Shindell, D. T., Sillman, S., Skeie, R. B., Spracklen, D., Stavrakou, T., Steenrod, S. D., Takemura, T., Tiitta, P., Tilmes, S., Tost, H., van Noije, T., van Zyl, P. G., von Salzen, K., Yu, F., Wang, Z., Zaveri, R. A., Zhang, H., Zhang, K., Zhang, Q., and Zhang, X.: The AeroCom evaluation and intercomparison of organic aerosol in global models, Atmospheric Chemistry and Physics, 14, 10 845–10 895, https://doi.org/10.5194/acp-14-10845-2014, 2014.

Viana, M., Pey, J., Querol, X., Alastuey, A., de Leeuw, F., and Lükewille, A.: Natural sources of atmospheric aerosols influencing air quality across Europe, Science of The Total Environment, 472, 825–833, https://doi.org/10.1016/j.scitotenv.2013.11.140, 2014.

Volkamer, R., Jimenez, J. L., San Martini, F., Dzepina, K., Zhang, Q., Salcedo, D., Molina, L. T., Worsnop, D. R., and Molina, M. J.: Secondary organic aerosol formation from anthropogenic air pollution: Rapid and higher than expected, Geophysical Research Letters, 33, https://doi.org/10.1029/2006GL026899, 2006.

Wang, P., Bi, S. P., Zhou, Y. P., Tao, Q. S., Gan, W. X., Xu, Y., Hong, Z., and Cai, W. S.: Study of aluminium distribution and speciation in atmospheric particles of different diameters in Nanjing, China, Atmospheric Environment, 41, 5788–5796, https://doi.org/10.1016/j.atmosenv.2007.01.064, 2007.

Weingartner, E., Nyeki, S., and Baltensperger, U.: Seasonal and diurnal variation of aerosol size distributions (10<D<750 nm) at a high-alpine site (Jungfraujoch 3580 m asl), Journal of Geophysical Research: Atmospheres, 104, 26 809–26 820, https://doi.org/10.1029/1999JD900170, 1999.

Yang, Y., Shao, M., Wang, X., Nölscher, A. C., Kessel, S., Guenther, A., and Williams, J.: Towards a quantitative understanding of total OH reactivity: A review, Atmospheric Environment, 134, 147–161, https://doi.org/10.1016/j.atmosenv.2016.03.010, 2016.

Ye, C., Lu, K., Song, H., Mu, Y., Chen, J., and Zhang, Y.: A critical review of sulfate aerosol formation mechanisms during winter polluted periods, Journal of Environmental Sciences, 123, 387–399, https://doi.org/10.1016/j.jes.2022.07.011, 2023.

Yu, H., Kaufman, Y. J., Chin, M., Feingold, G., Remer, L. A., Anderson, T. L., Balkanski, Y., Bellouin, N., Boucher, O., Christopher, S., DeCola, P., Kahn, R., Koch, D., Loeb, N., Reddy, M. S., Schulz, M., Takemura, T., and Zhou, M.: A review of measurement-based assessments of the aerosol direct radiative effect and forcing, Atmospheric Chemistry and Physics, 6, 613–666, https://doi.org/10.5194/acp-6-613-2006, 2006.

Zanatta, M., Gysel, M., Bukowiecki, N., Müller, T., Weingartner, E., Areskoug, H., Fiebig, M., Yttri, K. E., Mihalopoulos, N., Kouvarakis, G., Beddows, D., Harrison, R. M., Cavalli, F., Putaud, J. P., Spindler, G., Wiedensohler, A., Alastuey, A., Pandolfi, M., Sellegri, K., Swietlicki, E., Jaffrezo, J. L., Baltensperger, U., and Laj, P.: A European aerosol phenomenology-5: Climatology of black carbon optical properties at 9 regional background sites across Europe, Atmospheric Environment, 145, 346–364, https://doi.org/10.1016/j.atmosenv.2016.09.035, 2016.

Zanis, P., Monks, P. S., Schuepbach, E., and Penkett, S. A.: The Role of In Situ Photochemistry in the Control of Ozone during Spring at the Jungfraujoch (3,580 m asl) – Comparison of Model Results with Measurements, Journal of Atmospheric Chemistry, 37, 1–27, https://doi.org/10.1023/A:1006349926926, 2000.

Zarzycki, C. M. and Bond, T. C.: How much can the vertical distribution of black carbon affect its global direct radiative forcing?, Geophysical Research Letters, 37, https://doi.org/10.1029/2010GL044555, 2010.

Zellweger, C., Ammann, M., Buchmann, B., Hofer, P., Lugauer, M., Rüttimann, R., Streit, N., Weingartner, E., and Baltensperger, U.: Summertime NOy speciation at the Jungfraujoch, 3580 m above sea level, Switzerland, Journal of Geophysical Research: Atmospheres, 105, 6655–6667, https://doi.org/10.1029/1999JD901126, 2000.

https://doi.org/10.5194/egusphere-2026-3660
Preprint. Discussion started: 7 July 2026

Zellweger, C., Forrer, J., Hofer, P., Nyeki, S., Schwarzenbach, B., Weingartner, E., Ammann, M., and Baltensperger, U.: Partitioning of reactive nitrogen (NO_y) and dependence on meteorological conditions in the lower free troposphere, Atmospheric Chemistry and Physics, 3, 779–796, https://doi.org/10.5194/acp-3-779-2003, 2003.

Zheng, B., Chevallier, F., Yin, Y., Ciais, P., Fortems-Cheiney, A., Deeter, M. N., Parker, R. J., Wang, Y., Worden, H. M., and Zhao, Y.: Global atmospheric carbon monoxide budget 2000–2017 inferred from multi-species atmospheric inversions, Earth System Science Data, 11, 1411–1436, https://doi.org/10.5194/essd-11-1411-2019, 2019.

Zografou, O., Gini, M. I., Manousakas, M. I., Foskinis, R., Granakis, K., Fetfatzis, P., Diapouli, E., Papayannis, A., Nenes, A., and Eleftheriadis, K.: Aerosol Chemical Characterization and Seasonal Variability at the Helmos Hellenic Atmospheric Aerosol and Climate Change Mountain Station, Journal of Geophysical Research: Atmospheres, 130, e2025JD044 330, https://doi.org/10.1029/2025JD044330, 2025.